Numerical Simulation of Store Separation for Quasi-Steady Flow

TORSTEN BERGLIND

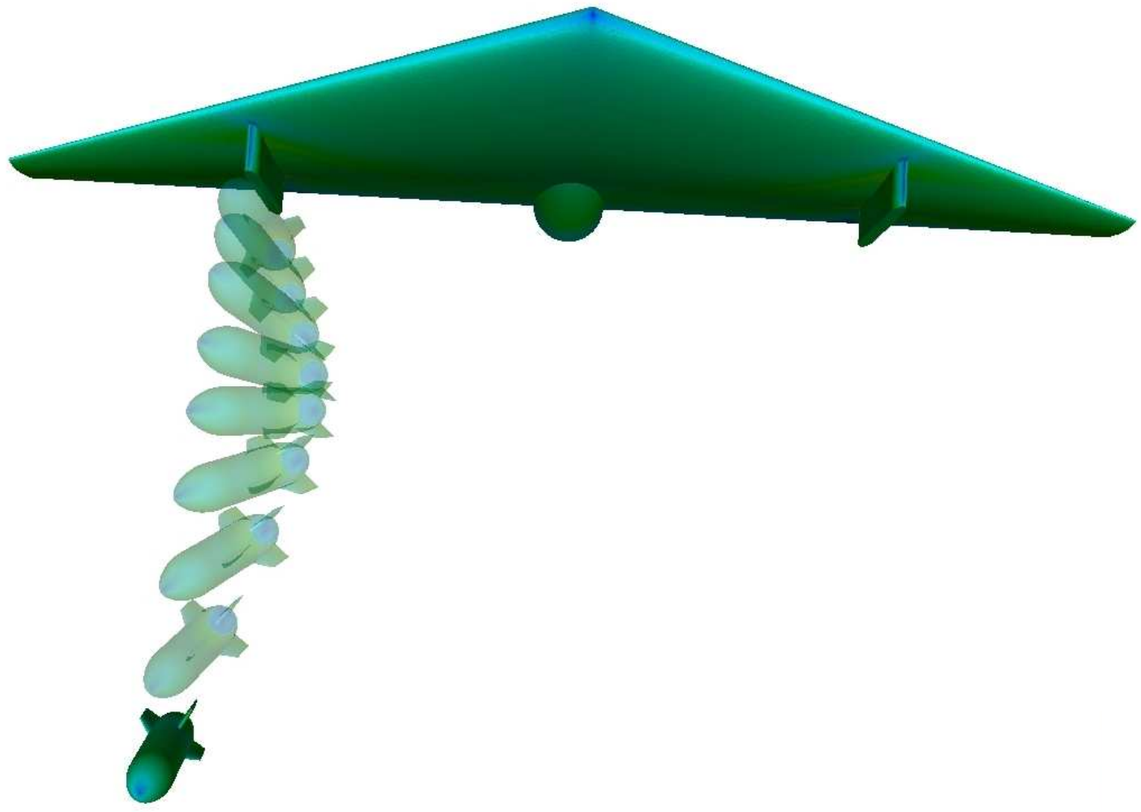

FOI
Defence Research Agency
Defence & Security, Systems and Technology
SE-164 90 Stockholm

Phone: +46 8 555 030 00
Fax: +46 8 555 031 00

www.foi.se

FOI-R--2761--SE Technical report
ISSN 1650-1942 May 2009

Defence & Security, Systems and Technology

Torsten Berglind

Numerical Simulation of Store Separation for Quasi-Steady Flow

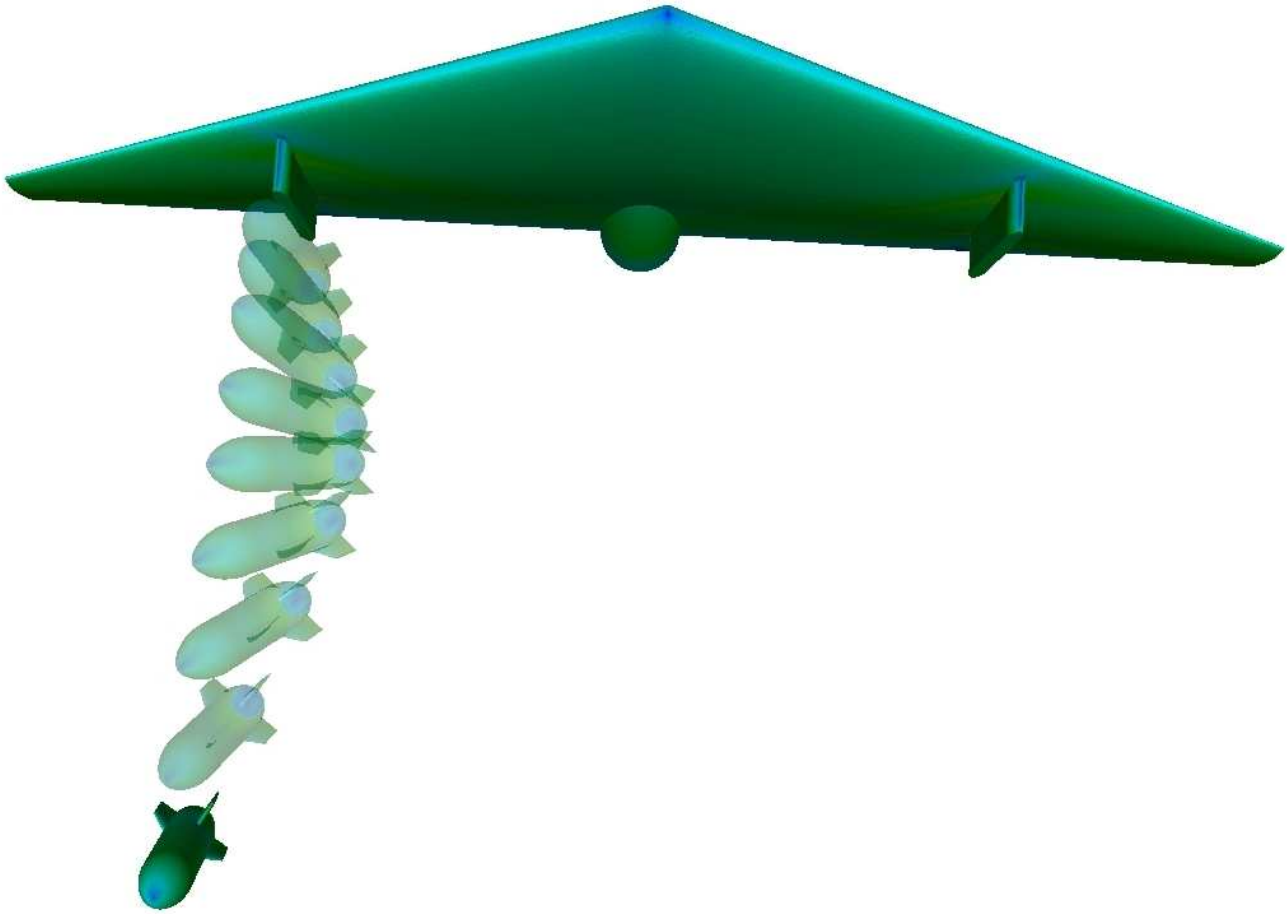

Titel	Numerisk simulering av lastseparation för kvasistationär strömning
Title	Numerical Simulation of Store Separation for Quasi-Steady Flow
Rapportnr/Report no	FOI-R--2761--SE
Rapporttyp Report Type	Teknisk rapport/Technical Report
Sidor/Pages	58 p
Månad/Month	Maj/May
Utgivningsår/Year	2009
ISSN	ISSN 1650-1942
Kund/Customer	FMV
Forskningsområde Programme area	5. Bekämpning och skydd/Strike and Protection
Delområde Subcategory	55 Flygteknik/Aeronuatics
Projektnr/Project no	E61351
Godkänd av/Approved by	Maria Sjöblom

FOI, Totalförsvarets Forskningsinstitut
Avdelningen för Försvars- och säkerhetssystem
164 90 Stockholm

FOI, Swedish Defence Research Agency
Defence & Security, Systems and Technology
SE-164 90 Stockholm

Sammanfattning

Huvudsyftet med FoT25-projektet ”Studier av inre vapenutrymme” har varit att bygga upp kunskap om effekter av instationär strömning på flygpestanda, på vapenschakt och på separationsbanor. Ett av de långsiktiga delmålen är att kunna prediktera fallbanor för laster från vapenschakt vilket oftast innebär instationära strömningsförhållanden. I denna rapport beskrivs en metod att göra kvasistationära beräkningar för separation av extern last. Ett integrerat system för simulering av separationsförlopp med strömningslösaren Edge har utvecklats. Beräkningar av kvasistationär strömning har kopplats till en flygmekanisk modell och den relativa rörelsen mellan flygplan och last har avbildats med en sekvens av deformerade och omgenererade nät. Den flygmekaniska modellen består av ekvationssystemet för en stelkroppsrörelse som löses med ett 5:e ordningens Runge-Kutta-schema. Den flygmekaniska modellen verifierades mot analytiska testfall och befanns ge mer än tillräcklig noggrannhet för typiska separationsbanor. För att validera implementationen av systemet för vapenseparationsbanor, beräknades ett AGARD-fall för separation av extern last. En fenförsedd missil separerades från en generisk vinge-sting-pylon-konfiguration med hjälp av en ERU(Eject Release Unit). Beräknad separationsbana och attitydvinklar stämmer bra med experiment.

Nyckelord: lastfällning, vapenschakt, instationär strömning, stelkroppsmodell

Summary

The main purpose of the FoT25-project “Studies of weapons bays” project has been to gain knowledge about the impact of unsteady flow around weapons bays on flight performance, on the cavity walls and on store separation trajectories. One of the long term goals is to be able to predict trajectories for stores from weapons bays usually implying unsteady flow conditions. In this report a method for computations of separation of an external store assuming quasi-steady flow conditions is presented. An integrated system for store separation simulations with the flow solver Edge has been developed. Computations of quasi-steady flow have been directly coupled to a flight mechanics model and the relative movement between the aircraft and the store are mapped by a sequence of deformed and remeshed grids. The flight mechanics model consists of the equations for rigid body motion solved by a fifth order Runge-Kutta scheme. The flight mechanics model was verified against analytical test cases demonstrating that the accuracy is more than sufficient to compute typical store separation trajectories. In order to validate the implementation of the system for store separation computations, an AGARD-test case for external store separation was computed. A finned missile is separated from a generic wing-sting-pylon configuration with use of an ERU (Eject Release Unit). The computed trajectories and attitudes agree well with experiment.

Keywords: Store separation, Weapons Bays, Unsteady Flow, Rigid Body-model

Contents

Nomenclature

C_{lp}, C_{mq}, C_{nr}	Aerodynamic damping coefficients
$\vec{F}$	Resultant force
I	Inertia tensor
$\vec{L}$	Resultant moment
m	Store mass
M	Mach number
$\vec{M}_d$	Aerodynamic damping moment
$M'_{Ld}, M'_{Md}, M'_{Gd}$	Moments due to aerodynamic damping
P, Q, R	Store roll, pitch and yaw rate
q	Dynamic pressure
Q	Transformation matrix
$\vec{r}$	Position vector
Re	Reynolds number
t	Time
V	Velocity
X, Y, Z	Flight-axis system: X in positive direction of flight path, Y positive to pilot's right, Z is positive downward
ϕ	Store roll angle, positive right wing down
θ	Store pitch angle, positive right wing down
ψ	Store yaw angle, positive nose right
$\dot{\psi}, \dot{\theta}, \dot{\phi}$	Angular rates
$\vec{\Omega}$	Rotation vector
Ω	Rotation matrix
$\vec{\omega}$	Angular velocity
$\dot{\vec{\omega}}$	Angular acceleration
A	Angle-of-Attack (AoA)

Subscript:

C	Mass centre
x, y, z	Component
∞	Free stream value

Superscript:

´	Moving reference system

1 Introduction

Each time an aircraft needs to carry and employ new stores it requires an airworthiness certification. Generally there are three tools that have been used: Wind tunnel Testing, CFD (Computational Fluid Dynamics) analyses and Flight testing. Today an integrated approach that uses the best features of the three approaches is the most frequently used. Analysis of store separation trajectories for external loads usually can be carried out successfully using the assumption of quasi-steady flow [1, 2 and 19].

Weapons bays are used to improve the aircraft aerodynamic performance and low observable characteristics. If the unsteady effects of the flow on the trajectories are significant, wind tunnel tests are of limited use since it's not possible to simultaneously capture all dimensionless parameters characterising the physical processes. Flight clearance procedures for unsteady flow conditions have to be extremely conservative since the trajectories will not be repeatable [6-9].

The main purpose of the FoT25-project "Studies of weapons bays" project has been to gain knowledge about the impact of unsteady flow around the weapons bay on flight performance, on the cavity walls and on store separation trajectories. A long term goal is to be able to predict trajectories for unsteady flow conditions. Accurate simulation of three-dimensional, time dependent, compressible flows about moving bodies, such as store separation from flight vehicles requires simultaneous modelling of several physical processes. Numerical modelling of these phenomena involves development of methodology to simulate the motion of complex geometry, three-dimensional bodies embedded in external, temporally and spatially evolving flows.

In the present work, quasi-steady approach is used to model the motion of separating an external store relative to its parent aircraft, using steady Euler flow computations, adding effects of aerodynamic damping. The implementation of a 6DOF (six degree of freedom) flight mechanics model for rigid bodies and its coupling to CFD is presented. The CFD-tool used is the FOI developed multi-purpose flow solver Edge [10]. The strategy for modelling moving bodies involves ALE (Arbitrary Lagrangian-Eulerian) methodology on unstructured grids [1,3,4 and 5]. The grid movement is modelled by a combination of grid deformation and remeshing, interpolating preceding solutions from previous grid levels onto successive grids [11].

The implementation for quasi-steady computations is done in a general code structure suited also for the implementation of unsteady flow computations. Simulation of trajectories for external carriage store separation is a major step towards simulation of store separation computations for unsteady flow. It also serves as validation of newly implemented modules: flight mechanics model, the grid modification routines, computation of the integrated store forces and moments, etc.

The general ALE methodology enables solutions of a new class of flow problems. Examples of possible applications are canopy and pilot ejection, fuel tank separation, rocket stage separation, shroud removal for interceptors and torpedo launches. The trend to push the flight performance and the use of unconventional configurations leads to flight mechanics instabilities dominated by non-linear behaviour of the flow. The simulation of this type of nonconventional motions requires simulations with flight mechanics directly coupled to CFD.

.

2 Flight Mechanics-model

The flight mechanics model is one of the crucial parts in a system for trajectory computations. Since it is also a new part of the Edge-system, it will be described thoroughly in this chapter. The moving object will be described as a rigid body, also denoted as a 6 DOF -model.

2.1 Equations of motion for a rigid body

According to the Euler's laws [12,13], the motion of a rigid body can be determined as,

$$\vec{F} = m\ddot{\vec{r}}_C \tag{2-1}$$

$$\vec{L}_C = \frac{d}{dt}(\vec{\omega} I_C) \tag{2-2}$$

where $\vec{F}$ is the resultant force on the body, m is the mass, $\vec{r}_C$ is the position vector to the mass centre, t is the time, $\vec{L}_C$ is the resultant moment relative to the mass centre, $\vec{\omega}$ is the angular velocity, and I_C is the inertia tensor with respect to the mass centre.

Equations (2-1) and (2-2) are valid in an inertial frame, that is a frame that moves with a constant velocity vector and without rotation. If we compute the inertia tensor I_C in this fixed frame as the body moves, then the inertia tensor will change with time. However, if we compute the inertia tensor with respect to body fixed axes I'_C, this tensor will be constant in time.

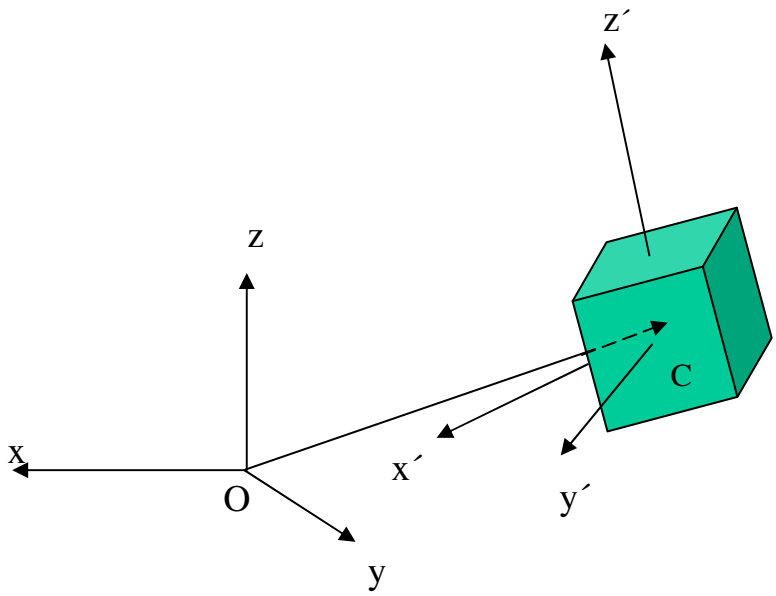

Figure 1 Introduction of a body fixed coordinate system.

The operator [12],

$$\frac{d}{dt} = \frac{D}{Dt} + \vec{\omega}\times \tag{2-3}$$

gives the relation between the time derivative in the fixed reference frame $\frac{d}{dt}$, and the time derivative in the body fixed reference frame $\frac{D}{Dt}$. The operand on the right hand side in equation (2-3) should be expressed in the body fixed moving reference frame. If we apply equation (2-3) on $\vec{\omega}$, it follows

$$\frac{d}{dt}\vec{\omega} = \frac{D}{Dt}\vec{\omega}' \tag{2-4}$$

where ´ denotes the moving reference frame. Hence, the rate of change of $\vec{\omega}$ relative to both reference systems is the same. Insertion of equation (2-4) in equation (2-2) and the fact

$$\frac{D}{Dt} I_C' = 0$$

leads to,

$$\begin{aligned} \vec{L}_C' &= \frac{d}{dt}(\vec{\omega}' I_C') = \frac{D\vec{\omega}'}{Dt} I_C' + \vec{\omega}' \frac{D}{Dt} I_C' + \vec{\omega}' \times (\vec{\omega}' I_C') = \\ &= \dot{\vec{\omega}}' I_C' + \vec{\omega}' \times (\vec{\omega}' I_C') \end{aligned} \tag{2-5}$$

Note that in this equation, everything is expressed in the moving store frame . By rewriting Eqn. (2-2) for a body fixed coordinate system, the inconveniance of time dependency for the interia tensor is cicumvented. However a new difficulty has arised, on the left-hand side, the applied moments must be described in terms of coordinate axis whose orientation are yet to be determined.

2.2 Integration of the equations of motion

Each time step the arodynamic forces and moments are computed. In order to compute the velocity and position of the mass centre, the equations of motion are integrated over each time step Δt. Integration of the force equation (2-1) with respect to time yields,

$$\dot{\vec{r}}_C(t) = \int_{t_0}^{t} \frac{\vec{F}}{m} dt + \dot{\vec{r}}_C(t_0) \tag{2-6}$$

where $\dot{\vec{r}}_C(t)$ and $\vec{r}_C(t)$ is the velocity and position of the mass centre, t is the time at the new time step and t_0 is the time at the previous time step.
The moment equation (2-5) is a coupled set of ordinary differential equations whose solution yields the components of the angular velocity of the body

$$\begin{pmatrix} L'_{Cx} \\ L'_{Cy} \\ L'_{Cz} \end{pmatrix} = \begin{pmatrix} I'_{xx} & I'_{xy} & I'_{xz} \\ I'_{xy} & I'_{yy} & I'_{yz} \\ I'_{xz} & I'_{yz} & I'_{zz} \end{pmatrix} \begin{pmatrix} \dot{\omega}'_x \\ \dot{\omega}'_y \\ \dot{\omega}'_z \end{pmatrix} + \begin{pmatrix} \omega'_x \\ \omega'_y \\ \omega'_z \end{pmatrix} \times \left(\begin{pmatrix} I'_{xx} & I'_{xy} & I'_{xz} \\ I'_{xy} & I'_{yy} & I'_{yz} \\ I'_{xz} & I'_{yz} & I'_{zz} \end{pmatrix} \begin{pmatrix} \omega'_x \\ \omega'_y \\ \omega'_z \end{pmatrix} \right) \tag{2-7}$$

If the body fixed axes are chosen as the principal axes with respect to the centre of mass, the products of inertia $I'_{xy}=I'_{yz}= I'_{zx}=0$, and equation (2-7) leads to,

$$\begin{pmatrix} \dot{\omega}'_x \\ \dot{\omega}'_y \\ \dot{\omega}'_z \end{pmatrix} = \begin{pmatrix} \frac{1}{I'_{xx}}(L'_{Cx} + (I'_{yy} - I'_{zz})\omega'_y\omega'_z) \\ \frac{1}{I'_{yy}}(L'_{Cy} + (I'_{zz} - I'_{xx})\omega'_x\omega'_z) \\ \frac{1}{I'_{zz}}(L'_{Cz} + (I'_{xx} - I'_{yy})\omega'_y\omega'_y) \end{pmatrix} \tag{2-8}$$

The equation (2-8) is usually denoted as Euler's equations of motion. Within a time step everything on the right hand side in equation (2-8), except the components of the angular velocity, will be considered to be constant.

The aim is to compute the new position of the body fixed coordinate system. From the time integration point of view, the most appropriate is to express the rotation of the body in terms of the vector $\vec{\Omega}$ which is directed along the rotation axis and its magnitude is α, the rotation angle. Since successive rotations are not commutative, $\vec{\Omega}$ does not qualify as a vector. However it can be shown that infinitesimal rotations $d\vec{\Omega}$ have the correct transformation properties under an orthogonal transformation.

The rotation of a vector with an angle α about a general axis $\vec{u}$ through the origin can be expressed by the rotation matrix Ω [14],

$$\Omega = \begin{pmatrix} u_1^2 + (1-u_1^2)\cos\alpha & u_1u_2(1-\cos\alpha) - u_3\sin\alpha & u_3u_1(1-\cos\alpha) + u_2\sin\alpha \\ u_1u_2(1-\cos\alpha) + u_3\sin\alpha & u_2^2 + (1-u_2^2)\cos\alpha & u_2u_3(1-\cos\alpha) - u_1\sin\alpha \\ u_3u_1(1-\cos\alpha) - u_2\sin\alpha & u_2u_3(1-\cos\alpha) + u_1\sin\alpha & u_3^2 + (1-u_3^2)\cos\alpha \end{pmatrix} \quad (2\text{-}9)$$

The inverse transformation from body coordinates to the reference frame is, since Ω is an orthogonal matrix, given by the transposed matrix Ω^*.

$$\vec{a} = \Omega^{-1}\vec{a}' = \Omega^*\vec{a}' \quad (2\text{-}10)$$

where $\vec{a}$ is an arbitrary vector.

The time derivative of $\vec{\Omega}$ is defined as the angular velocity $\vec{\omega}$,

$$\dot{\vec{\Omega}} = \frac{d\vec{\Omega}}{dt} = \vec{\omega} \quad (2\text{-}11)$$

Equations (2-1), (2-6), (2-8) and (2-11) constitutes a set of coupled ordinary differential equations with constant coefficients that constitutes the system of 12 ordinary differential equations to be solved.

$$\vec{q} = \begin{pmatrix} \dot{\vec{r}}_C \\ \vec{r}_C \\ \vec{\omega}' \\ \vec{\Omega}' \end{pmatrix} \quad (2\text{-}12)$$

$$\dot{\vec{q}} = \vec{f}(\vec{q})$$

where $\vec{f}$ is the right hand side of the corresponding equations.

Integration of equation (2-12) in time is done with a fifth order accurate Runge-Kutta method RKF45 (Runge-Kutta-Fehlberg) [15], see appendix A and equation (A-1).

2.3 The movement expressed in Cardan angles

Since the elements of the rotation matrix are not independent, they are not suitable as generalized coordinates. A number of sets of independent variables for describing the motion of a stiff body have been described in the litterature. The standard way to describe the rotational movement for store release is to use Cardan angles. Cardan angles imply succesive rotations about the three body fixed coordinate axes, first the z-axis, then the y-axis and finally the x-axis. Cardan angles are often denoted Euler angles in flight mechanics litterature.

A standard way of orienting the coordinate system is: z-axis downwards, x directed along the body axis and y perpendicular to the body axis, see figure 2. The Cardan angles for this coordinate system wlll be oriented as:

ψ is the body axis yaw angle, positive nose right

θ is the body axis pitch angle, positive nose up

ϕ is the body roll angle, positive right wing down

In flight mechanics contexts [16] the Cardan angles are often limited to a periodic interval,

$$\psi \in [-\pi, \pi[\qquad \psi \in [0, 2\pi[$$
$$\theta \in \left[-\frac{\pi}{2}, \frac{\pi}{2}\right] \quad \text{or} \quad \theta \in \left[-\frac{\pi}{2}, \frac{\pi}{2}\right]$$
$$\phi \in [-\pi, \pi[\qquad \phi \in [0, 2\pi[$$

It will now be shown that the elements of the orthogonal transformation can be expressed in terms of theese angles.

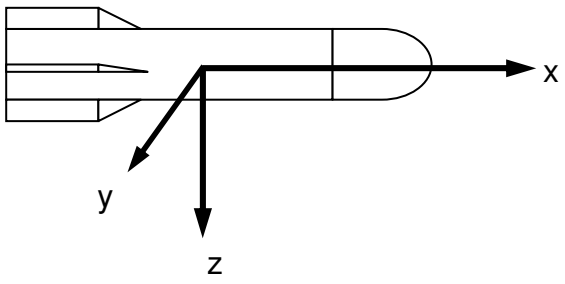

Figure 2. Orientation of the body axis coordinate system

The sequence of rotations starts with a counterclockwise rotation around the z-axis,

$$Q_\psi = \begin{pmatrix} \cos\psi & \sin\psi & 0 \\ -\sin\psi & \cos\psi & 0 \\ 0 & 0 & 1 \end{pmatrix} \tag{2-13}$$

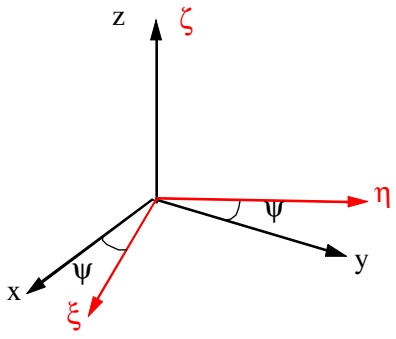

Figure 3. Rotation around the z-axis.

The resultant coordinate system is labelled $\xi,\eta,\zeta-$ axis. In the next step this coordinate system is rotated counterclockwise an angle θ about the η-axis

$$Q_\theta = \begin{pmatrix} \cos\theta & 0 & -\sin\theta \\ 0 & 1 & 0 \\ \sin\theta & 0 & \cos\theta \end{pmatrix} \tag{2-14}$$

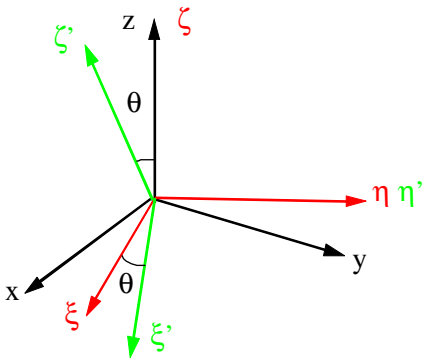

Figure 4. Rotation around the y-axis.

This intermediate set of axis is denoted ξ',η',ζ'. Finally, the ξ',η',ζ' axes are rotated counterclockwise an angle ϕ around the ξ'-axis

$$Q_\phi = \begin{pmatrix} 1 & 0 & 0 \\ 0 & \cos\phi & \sin\phi \\ 0 & -\sin\phi & \cos\phi \end{pmatrix} \tag{2-15}$$

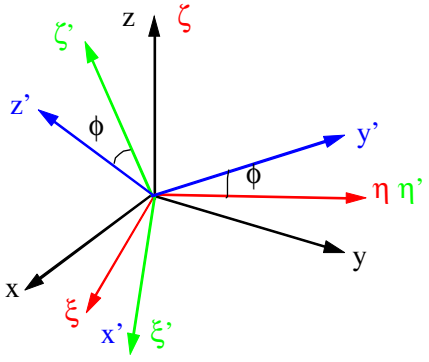

Figure 5. Rotation around the x-axis.

Finally the desired system of axes x´,y´,z´ is obtained.

The complete transformation Q can be obtained by writing the matrix as a product of three separate rotations,

$$\begin{aligned} Q &= Q_\phi Q_\theta Q_\psi \\ \vec{a}' &= Q\vec{a} \\ \vec{a} &= Q^{-1}\vec{a}' \end{aligned} \tag{2-16}$$

where $\vec{a}$ is an arbitrary vector.

The transformation matrix Q then follows as

$$Q = \begin{pmatrix} \cos\theta\cos\psi & \cos\theta\sin\psi & -\sin\theta \\ -\cos\phi\sin\psi + \sin\phi\sin\theta\cos\psi & \cos\phi\cos\psi + \sin\phi\sin\theta\sin\psi & \sin\phi\cos\theta \\ \sin\phi\sin\psi + \cos\phi\sin\theta\cos\psi & -\sin\phi\cos\psi + \cos\phi\sin\theta\sin\psi & \cos\phi\cos\theta \end{pmatrix} \tag{2-17}$$

Each time step the rotation vector $\Delta\vec{\Omega}'$ describing the rotation during the time step is computed from equation (2-11). This vector is transformed to a rotation matrix $\Delta\Omega'$ using equation (2-9). In analogy with (2-15), the transformation matrix for the subsequent time step (k+1) becomes,

$$Q^{(k+1)} = \Delta\Omega' \cdot Q^{(k)} \tag{2-18}$$

where $Q^{(k)}$ is the previous transformation matrix. The new Cardan angles ψ, θ, ϕ can be determined by identification betweeen current rotational matrix, and Q in equation (2-17)

$$\begin{aligned} \psi &= \arctan\left(\frac{Q_{12}}{Q_{11}}\right) \\ \theta &= -\arcsin(Q_{13}) \\ \phi &= \arctan\left(\frac{Q_{23}}{Q_{33}}\right) \end{aligned}$$

If $\cos\theta = 0$ then Q_{11} and Q_{33} will be 0 and the expressions above invalid. In this case ψ and ϕ can, for example, be evaluated from Q_{21} and Q_{31}. The representation Cardan angles have a so called gimbal lock for $\cos\theta = 0$ and it also is sensitive to errors. Gimbal lock is the phenomenon of two rotational axis of an object pointing in the same direction. Therefore, direction cosines of the transformation matrix Q are chosen to represent the solid angles. This has the drawback of requiring redundant information but the problem with gimbal lock and sensitivity to errors are circumvented. However in order to be able to plot the attitude we still have to compute the Cardan angles.

The position vector of an arbitrary P point on the surface of the solid body can from the movement of the centre of mass C and the rotation matrix Q be computed as,

$$\vec{r}_{p"} = \vec{r}_C + \vec{r}_{CC'} + Q\vec{r}_{C'P'} = \vec{r}_C + \vec{r}_{CC'} + Q\vec{r}_{CP} \tag{2-19}$$

where P" is the new position of P and C' is the new position of C, see Figure 6.

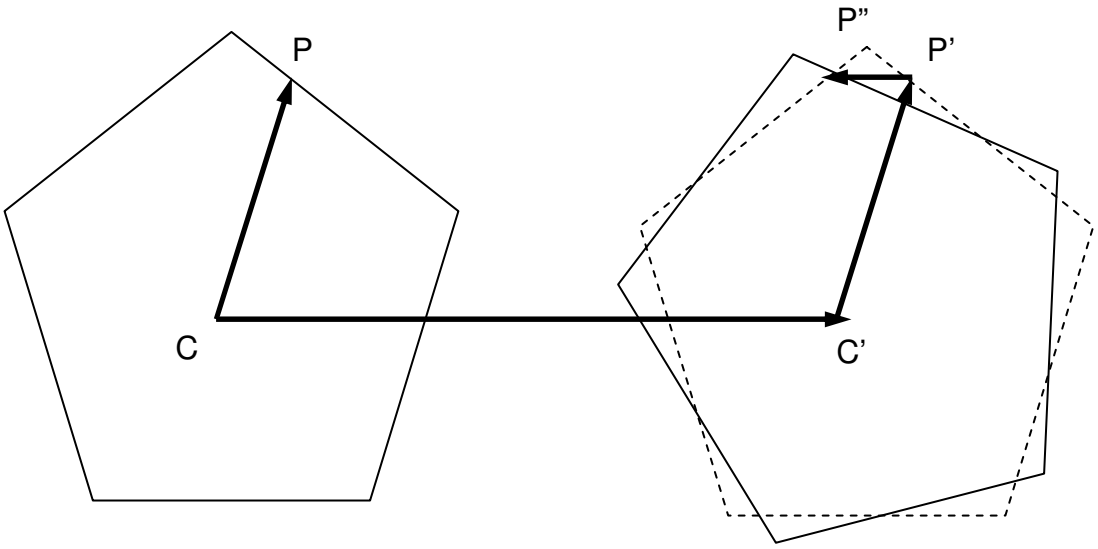

Figure 6. Movement of an arbitrary surface point P.

The angular velocity components can be related to the changes in orientation angles of the store reference frame ψ, θ and ϕ. Since $\vec{\omega}'_\psi$ is parallel with the z-axis, its component along the body axes are given by applying the tranformation matrix

$$\vec{\omega}'_\psi = Q\begin{pmatrix} 0 \\ 0 \\ \dot{\psi} \end{pmatrix} = \begin{pmatrix} -\dot{\psi}\sin\theta \\ \dot{\psi}\sin\phi\cos\theta \\ \dot{\psi}\cos\phi\cos\theta \end{pmatrix} \tag{2-20}$$

$\vec{\omega}'_\theta$ is parallel with the ξ'-axis and the components with respect to the body axes can be determined by applying only the final transformation Q_ϕ,

$$\vec{\omega}'_\theta = Q_\phi\begin{pmatrix} 0 \\ \dot{\theta} \\ 0 \end{pmatrix} = \begin{pmatrix} 1 & 0 & 0 \\ 0 & \cos\phi & \sin\phi \\ 0 & -\sin\phi & \cos\phi \end{pmatrix}\begin{pmatrix} 0 \\ \dot{\theta} \\ 0 \end{pmatrix} = \begin{pmatrix} 0 \\ \dot{\theta}\cos\phi \\ -\dot{\theta}\sin\phi \end{pmatrix} \tag{2-21}$$

No transformation is necessary for the components of $\vec{\omega}'_\phi$ which is directed along the x'-axis.

$$\vec{\omega}'_\phi = \begin{pmatrix} \dot{\phi} \\ 0 \\ 0 \end{pmatrix} \tag{2-22}$$

Adding the components of the separate angular velocities, equations, and the components of with respect to the body axes are,

$$\vec{\omega}' = \begin{pmatrix} \omega'_x \\ \omega'_y \\ \omega'_z \end{pmatrix} = \begin{pmatrix} -\dot{\psi}\sin\theta + \dot{\phi} \\ \dot{\psi}\sin\phi\cos\theta + \dot{\theta}\cos\phi \\ \dot{\psi}\cos\phi\cos\theta - \dot{\theta}\sin\phi \end{pmatrix} \tag{2-23}$$

The components ω'_x, ω'_y and ω'_z are called the rotation rates and are often denoted P, Q and R resectively [16,17].

Solving equation (2-23) for angular rates $\dot{\psi}, \dot{\theta}, \dot{\phi}$ yields,

$$\begin{pmatrix} \dot{\psi} \\ \dot{\theta} \\ \dot{\phi} \end{pmatrix} = \begin{pmatrix} \frac{1}{\cos\theta}(\omega'_y \sin\phi + \omega'_z \cos\phi) \\ \omega'_y \cos\phi - \omega'_z \sin\phi \\ \omega'_x + \tan\theta(\omega'_y \sin\phi + \omega'_z \cos\phi) \end{pmatrix} \tag{2-24}$$

The angular rates $\dot{\psi}, \dot{\theta}, \dot{\phi}$ are called the yaw rate, pitch rate and roll rate of the store, respectively.

2.4 Aerodynamic damping

Quasi-steady computations imply that the flow at each moment of the movement is considered as steady. In order to take the body's own movement into account, aerodynamic damping coefficients are applied [16]. The aerodynamic damping moment $\vec{M}'_d$ is computed as,

$$\vec{M}'_d = \begin{pmatrix} M'_{Ld} \\ M'_{Md} \\ M'_{Gd} \end{pmatrix}$$

$$M'_{Ld} = C_{lp} P b_r \frac{1}{2V_r} q_{dyn_r} S_r c_r \tag{2-25}$$

$$M'_{Md} = C_{mq} Q c_r \frac{1}{2V_r} q_{dyn_r} S_r c_r$$

$$M'_{Gd} = C_{nr} R c_r \frac{1}{2V_r} q_{dyn_r} S_r c_r$$

where M'_{Ld}, M'_{Md} and M'_{Gd} are components of the aerodynamic damping moment, C_{lp}, C_{mq} and C_{nr} are aerodynamic damping coefficients, P,Q, and R are the rotation rates, V_r is the velocity of the moving body, q_{dyn_r} is the dynamic pressure for the moving body, S_r is reference area, c_r is reference length and and b_r is reference span. The values of the aerodynamic damping coefficients C_{lp}, C_{mq} and C_{nr} are always negative.

The moment $\vec{M}'_d$ is expressed in the reference frame of the moving object. This moment is transformed to the aircraft reference system ,

$$\vec{M}_d = Q^{-1} \vec{M}'_d \tag{2-26}$$

and added to the moment on the store.

2.5 Test cases for the 6DoF model

2.5.1 **Rotation of a body around an arbitrary axis**

A body is at rest at t=0:

$\vec{r}_C = \vec{0}, \dot{\vec{r}}_C = \vec{0}, \psi = 0, \theta = 0, \phi = 0, \dot{\psi} = 0, \dot{\theta} = 0, \dot{\phi} = 0,$

See Figure 7. At time t=0 the gravity force $\vec{F} = (0.,0.,9.80665)$ and a constant force moment $\vec{L} = (\frac{1}{\sqrt{3}}, \frac{1}{\sqrt{3}}, \frac{1}{\sqrt{3}})$ start to act on the body. The principal moments of inertia is set to $I_1 = I_2 = I_3 = 1$.

Figure 11 demonstrates that the agreement between computed and analytical results of the rotational angles ψ, θ and ϕ is excellent. Also the angular rates show excellent agreement with analytical results, Figure 12. The angular rates $\dot{\psi}$ and $\dot{\theta}$ should be zero. Although the deviation from zero is increasing with the rotational movement it is for both angular rates within 10^{-7} radians after more than three revolutions.

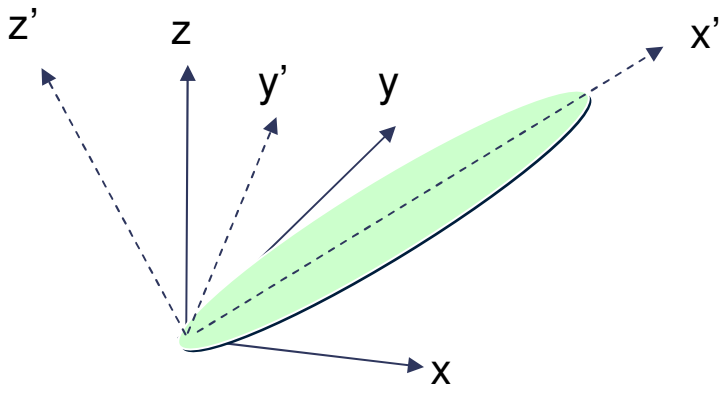

Figure 7. Rotational movement of a stiff body around an arbitrary axis.

For the computed trajectory coordinates x_C, y_C and z_C, the agreement with analytical results is within machine accuracy, Figure 13. Also the velocity components of the mass centre $\dot{x}_C$, $\dot{y}_C$ and $\dot{z}_C$ agree within machine accuracy with analytical results, Figure 14.

Usually the duration of a store separation scenario comprise less than 1 sec and the Cardan angles less than 90^o. The conclusion is therefore that the numerical method chosen for integration of the equations of the flight mechanics model fulfils the requirements of accuracy for simulation of store separation applications.

2.5.2 Precession movement of the angular velocity for a symmetrical rigid body

The angular velocity of a symmetrical rigid body can under force-free condition perform a precession movement. Let the symmetry axis be the z-axis, taken as principal axis so that $I_1 = I_2$. This leads to the solution [12] for the angular velocity in the body fixed system,

$$\omega'_x = A\sin\Omega t$$
$$\omega'_y = A\cos\Omega t$$
$$\omega'_z = \Omega\frac{I_1}{I_1 - I_3}$$

where Ω is the angular frequency, A is some constant and t the time. It should be noted that the precession described here is relative to the body axes, which are themselves rotating in space with another frequency ω.

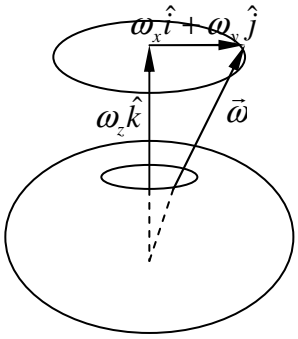

Figure 8. Precession of the angular velocity about the axis of symmetry in free-force motion of a symmetrical rigid body.

The initial conditions determine the angle θ between the angular velocity and the symmetry axis. If the angular velocity magnitude of is set to $|\vec{\omega}| = 2$, it follows that $\theta = \frac{\pi}{6}$. The initial conditions at t=0 for the Cardan angles are set to $\psi = 0$, $\theta = \frac{\pi}{6}$ and $\phi = 0$. Equation (2-24) gives the angular rates at t=0: $\dot{\psi} = 2$, $\dot{\theta} = 1$ and $\dot{\phi} = 1$. No force or moment is acting on the body. The principal moments of inertia is set to $I_3 = 3I_1 = 3I_2$, which determines the precession frequency to $\Omega = -2\sqrt{3}$.

In Figure 15 the computed vorticity components in the body fixed coordinate system are compared with the analytical expressions above. As in the previous example, there is a very good match between the analytical and the computed results. The rotational angles ψ, θ and ϕ and the angular rates $\dot{\psi}, \dot{\theta}$ and $\dot{\phi}$ are plotted versus time in Figure 16 and 17. The reason that the angular rates as a function of time are asymmetic is that they consists of superposition of two rotational movements with frequencies that are not even multiples of each other.

3 Implementation of flight mechanics model in Edge

3.1 Implementation

The implementation of a flight mechanics model in Edge includes modules for grid deformation, grid quality check, local remeshing [11] and interpolation of flow solutions between grids. From the flow solution, integrated forces of the moving object are computed and passed on to the flight mechanics model. A new position is computed and the coordinates of the new boundary points are sent to the grid deformation module. After the grid is adapted to the new position, the grid quality is checked. If the grid is OK, volumes and surfaces of the new grid are recomputed and a new flow solution is computed. If the grid quality is not OK, Edge is stopped and a new grid is computed, implying that a new dual grid has to be computed by the pre-processor.

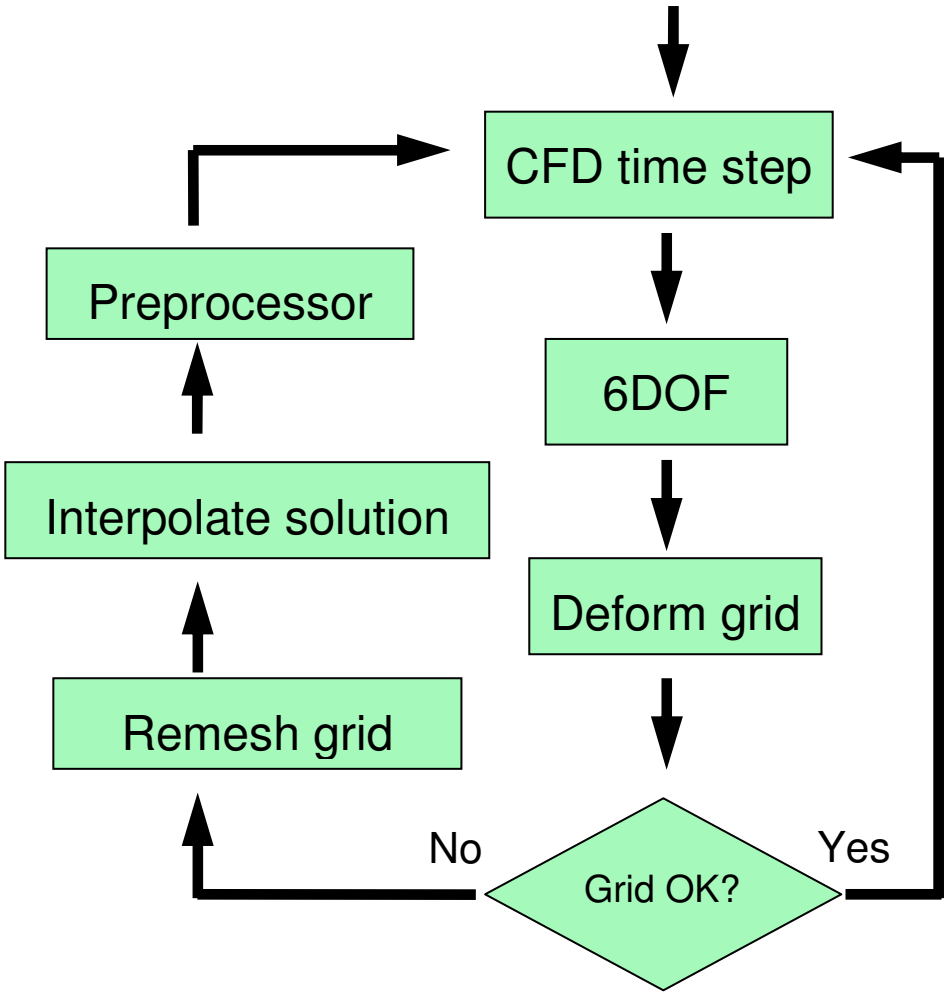

Figure 9. Flow chart of the trajectory computations coupled to the remeshing modules.

The computations proceeds until the desired number of iterations are computed.

The data flow to the flight mechanics model can be described as in Figure 10. A state vector consisting of the unknown variables in the system of equations to be solved is updated. The transformation matrix at time t, Q_t can be computed from the state vector but is stored separately in order to minimize the effect of round off errors.

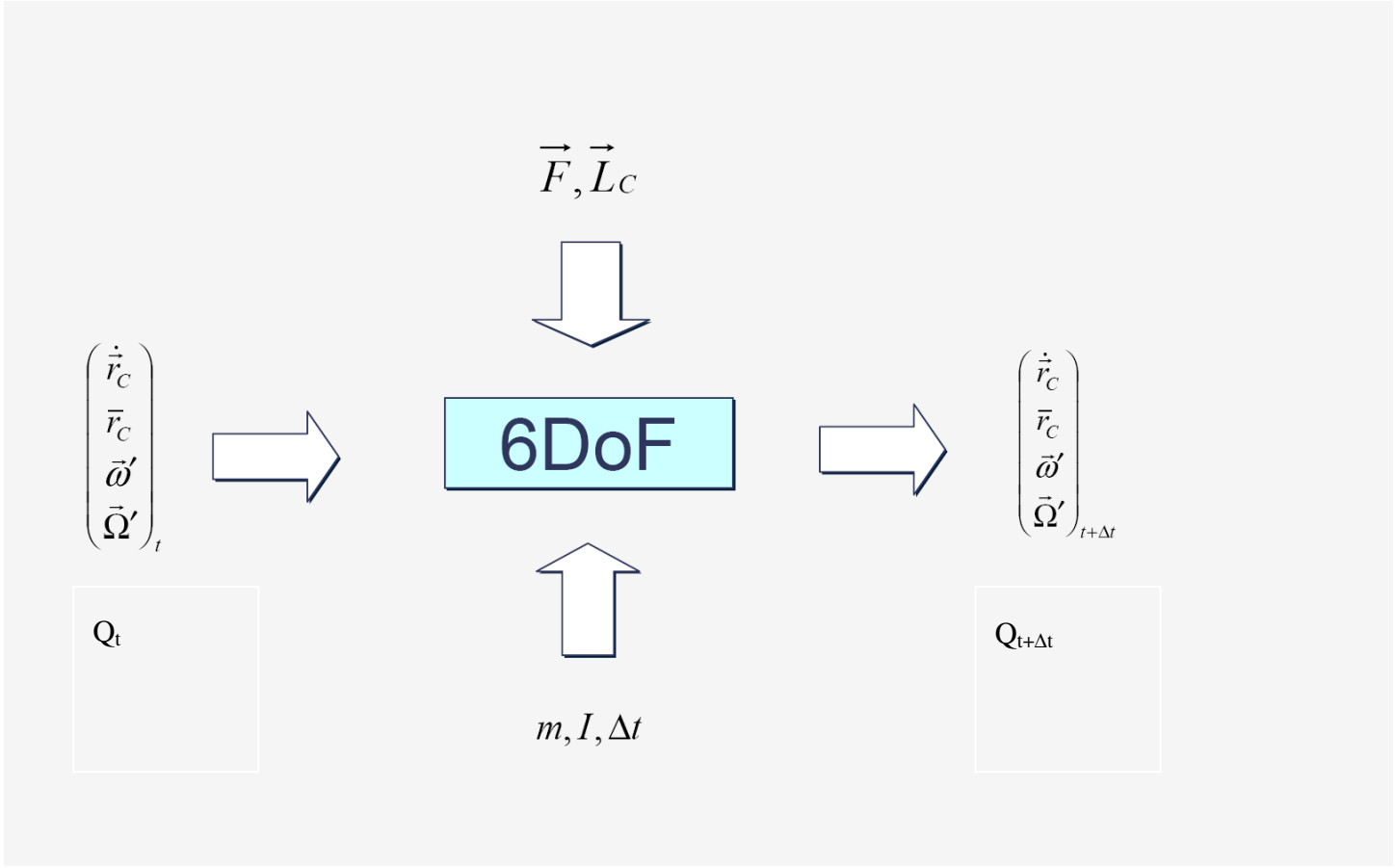

Figure 10. Data flow of the 6 DOF computations.

3.2 New parameters in the input file

Appendix B shows an example of the trajectory parameters in an input file. The parameter TRAJECTORY_DATA is a label for all trajectory data. The parameters are then divided into two parts: general parameters and parameters associated with a certain moving object. There are five general parameters:

`ITRAJEC` – flag 0 = no trajectory, 1 = quasi-steady computations, 2 = unsteady computations

`DELTAT_QS` – time step for quasi-steady computations

`GRAV` – gravitational vector

`NSUBST` - number of sub steps for 6DOF computations

`CHKMAX` – maximum grid stretching

It then follows a new label `TRAJECTORY` for each moving object. A moving object is specified with 16 parameters:

`b_traj_name` – the trajectory name

`b_names` – list of boundaries defining the moving object

MASS – object mass

INERT - the inertia tensor: Ixx, Iyy, Izz, Ixy, Ixz, Iyx

COOR0 - initial coordinates of the origo of the moving frame

COORC - coordinates of the store centre of mass in the moving frame

VC0 - initial velocity of the store centre of mass in the main frame

CARDAN - initial Cardan angles psi, teta, phi in radians

CARDANP - initial Cardan angular rates dpsi/dt, dteta/dt, dphi/dt in radians/s

DEFVEC - grid compression vector

CLP - roll damping coefficient

CMQ - pitch damping coefficient

CNR - yaw damping coefficient

RLENGTH - reference length

RSPAN - reference span

RAERA - reference area

The last six parameters are used to define the aerodynamic damping. Even if it is possible to define more than one moving object the current status of the local remeshing program allow only one moving object in the reference frame.

3.3 2D test case for trajectory computations

Store separation computations tend to be computationally demanding. It is therefore useful to have a 2D test case to check the development work on. The possibility to plot the grid has facilitated inspection of the grid generation techniques.

A 2D test case with two NACA0012 profiles was defined. The start position can be seen in Figure 18a. The upper profile is considered to correspond to the aircraft and the lower to the store.

The free stream values are:

$M_\infty = 0.800$, $p_\infty = 100000.0\ \mathrm{N/m^2}$, $T_\infty = 300\,\mathrm{K}$.

The standard gravity acceleration is $g = 9.80665\ \mathrm{m/sec^2}$. The mass of the store is

$M = 40000\,\mathrm{Kg}$

Inertia data

$$I_{xx} = 10000000 \text{ Kg m}^2$$
$$I_{yy} = 30000000 \text{ Kg m}^2$$
$$I_{zz} = 30000000 \text{ Kg m}^2$$

Roll, yaw and pitch damping coefficient

$$C_{lp} = -4.0/\text{rad}$$
$$C_{mq} = -40.0/\text{rad}$$
$$C_{nr} = -40.0/\text{rad}$$

An Euler grid with approximately 8000 nodes is generated. The initial position is shown in Figure 18 a. The grid is stretched more and more as the store moves downwards. In the position in Figure 18 b, the grid quality module stops further deformation of the grid and the grid merging program generates a new grid for the same position, Figure 18 c. The store moves further downwards in a rocking manner, see Figure 18 d. Four remeshings are sufficient to simulate the separation.

The cause for the rocking movement is that a shock is formed between the wing profiles, see Figure 19a. It resolves as the store is making a pitch down movement and a restoring moment is created, see Figure 19b. The store makes a pitch up movement and the shock between the wing profiles reappear and so forth, see Figure 19d. In Figure 20b, it can be noted that the profile is doing a damped sinusoidal pitch movement.

3.4 Store separation from a generic wing-sting-pylon configuration

In order to validate the implementation of a flight mechanics model in Edge, an AGARD test case carried out at AEDCs (Arnold Engineering Development Centre) 4-Foot Transonic Aerodynamic Wind Tunnel (4T) is chosen, see reference [19]. The test program was funded and supported by the AFRL (U.S. Air Force Research Laboratory).

A generic finned-store shape and a clipped delta wing with a 45 degree leading edge sweep were the primary test objects. The rig was positioned such that the store at carriage nearly touched the left or right pylons in the initial position, as required to initiate a trajectory, Figure 21 a.

The wind tunnel tests are carried out with CTS (Captive Trajectory System) technique. The store is attached to a separate sting that is moved with computer controlled motors. An online 6-DOF computer program solves equations of motion which gives next position for each step. The temporal steps to update the store positions are approximately 0.0002 seconds in pseudo time, falling store real time.

Runs in the wind tunnel were carried out with the store mounted on both left and right side of the wing. The available data corresponds to the store mounted on the right side of the wing. The flow case is hence asymmetric and therefore a full model is required for the computations.

The ERU (Ejection Release Unit) consists in this case of two pistons with the ejector stroke length 0.10 m which are released simultaneously. The forward ejection location is 1.24 m and the aft ejector location is positioned 1.75 m aft of the store nose. The forward ejector force is 10675.7 N and the aft ejector force is 42702.9N, both constant in time, see Figure 22. A model of the ERU is at the current stage of the not implemented in the code.

Since the primary goal was to validate the coupling of the flight mechanics model to CFD, it was decided to omit the part of the separation where the pistons are in physical contact with the store. The moment when the contact between the pistons and the store cease to occur, appear approximately 55 ms after it has left the original position. The computations are therefore started at the subsequent temporal measurement station, 60 ms after the store has left the original position, see Figure 21b. Thereby the ERU only influences the initial condition of the computations.

Two unstructured tetrahedral grids were generated around the aircraft with $5.7 \cdot 10^6$ nodes and around the missile with $0.20 \cdot 10^6$ nodes. The first grid was then coarsened outside the vicinity of the aircraft and away from the trajectory path to a grid with $1.8 \cdot 10^6$ nodes, Figure 23 and 24. The grids with both the aircraft and the missile in subsequent positions are then generated by a merge of the two grids using the local remeshing routine, see Figure 25.

The free stream entities for the wind –tunnel measurements are averaged over the test interval. Following free stream values was obtained:

$$M_\infty = 0.9511428\,, \quad p_\infty = 32071.64 \ \text{N/m}^2\,, \quad T_\infty = 259.7788\,\text{K}\,.$$

If the gas constant for air is set to R= 287 K m^2/s^2 it follows that

$$V_\infty = 307.2929 \ \text{m/s}$$

$$\rho_\infty = 0.4301655\,\text{Kg/m}^3$$

The standard gravity acceleration is $g = 9.80665 \ \text{m/sec}^2$. The mass of the store is

$$M = 907.1803317\,\text{Kg}$$

Inertia data

$$I_{xx} = 27.12\,\text{Kg m}^2$$

$$I_{yy} = 488.1\,\text{Kg m}^2$$

$$I_{zz} = 488.1\,\text{Kg m}^2$$

Roll, yaw and pitch damping coefficient

$$C_{lp} = -4.0/\text{rad}$$

$$C_{mq} = -40.0/\text{rad}$$

$$C_{nr} = -40.0/\text{rad}$$

First a steady computation is performed for the missile in its initial position. A quasi-steady computation is started and the grid is deformed every time step to conform to new positions. The grid quality is checked for each new grid and if it's not satisfactory the computation is stopped. A new grid is then generated with the local remeshing routine and the flow solution on the previous grid is interpolated onto the new grid. The computations continue until the specified number of iterations is computed. The whole procedure is managed by a shell-script.

In Figure 26 the aircraft and missile are depicted at two different temporal positions, t=0.15 and t=0.42 after the release. In Figure 27 and 28 the trajectory and attitude are plotted against time for various time step sizes, Δt = 0.01, 0.005 and 0.001sec. Figure 27 shows that there is an influence of the time step size on y_C, whereas for x_C and z_C the computational results are almost identical. Similarly, in Figure 28 there is an impact on ϕ with the time step size whereas the effects on ψ and θ are small. In the experiments, an online 6 DOF computer program solves equations of motion which gives next position of store using measured forces and moments as initial conditions for each step. The time step for updating the positions was 0.0002 s. In Figure 27b and Figure 28c it can be seen that y_C and ϕ approaches the experimental values as the time step is decreased.

In Figure 29 and 30 the trajectory and attitude with and without aerodynamic damping are plotted. It is clear from these plots that the influence of the aerodynamic damping in this case is small. Finally the results for $\Delta t = 0.001$ sec are plotted against experiments. Good agreement is achieved for both the trajectory and attitude, except for the roll angle. The results would improve further with a smaller time step. The agreement with experiments is almost as good as the reference computation in reference [19].

4 Figures

a.

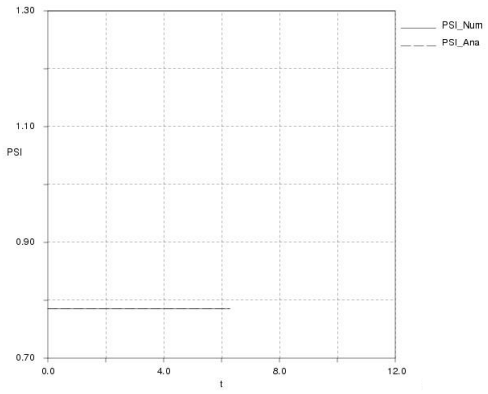

b.

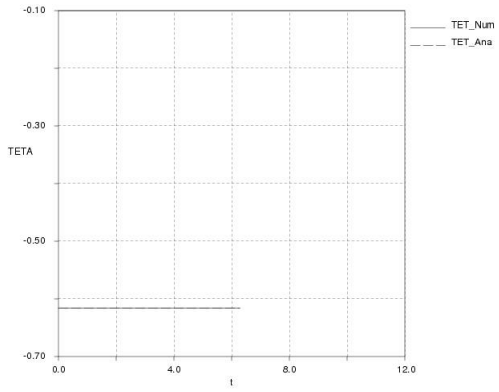

c.

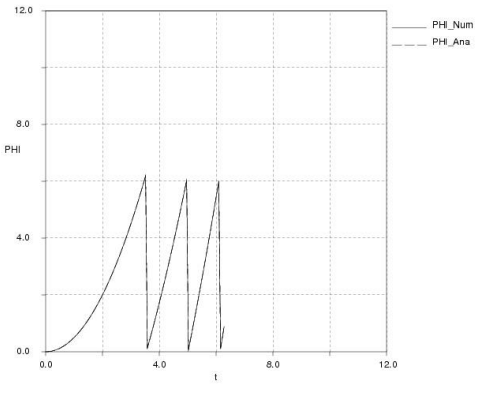

Figure 11. Rotational angles ψ, θ and ϕ as functions of time for test case 1.

a.

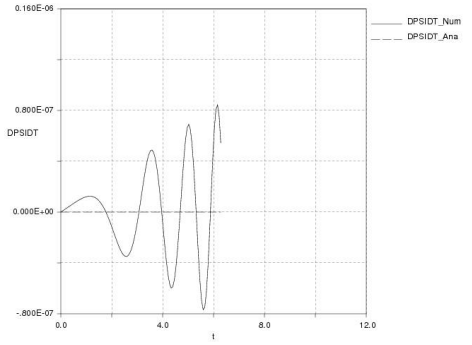

b.

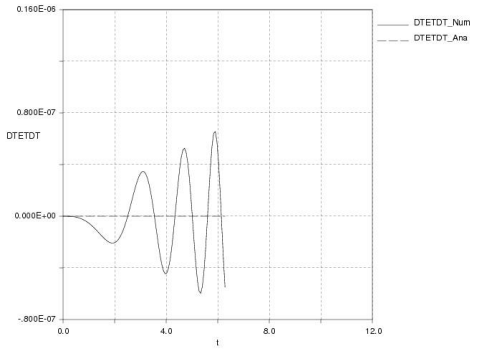

c.

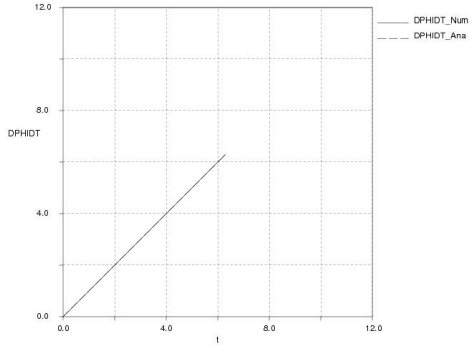

Figure 12. Angular rates $\dot{\psi}, \dot{\theta}$ and $\dot{\phi}$ as functions of time for test case 1.

a.

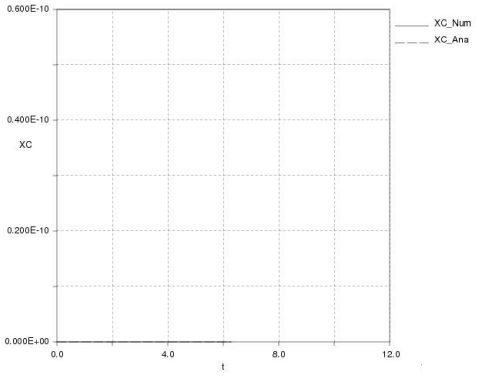

b.

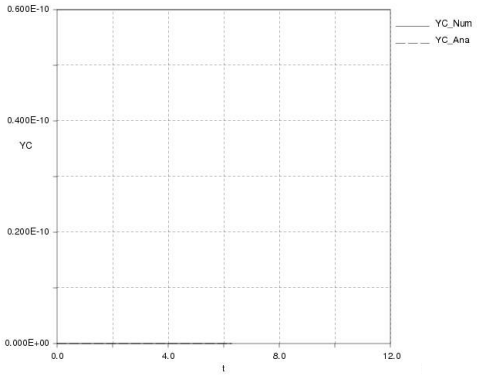

c.

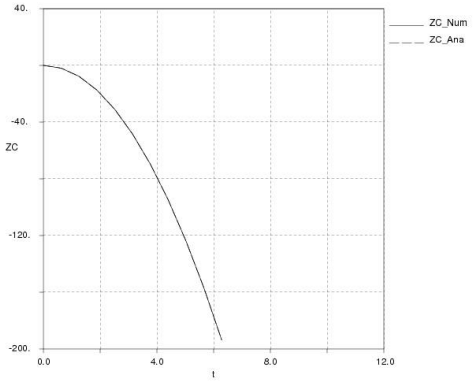

Figure 13. Position of the store mass centre x_C, y_C and z_C as functions of time for test case 1.

a.

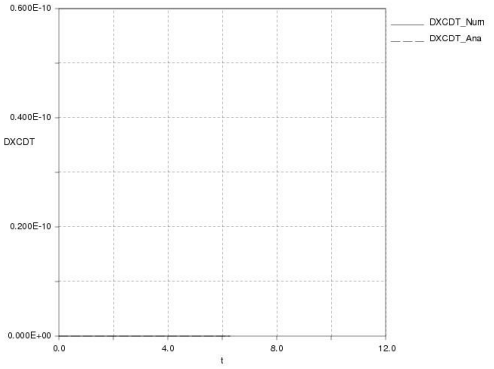

b.

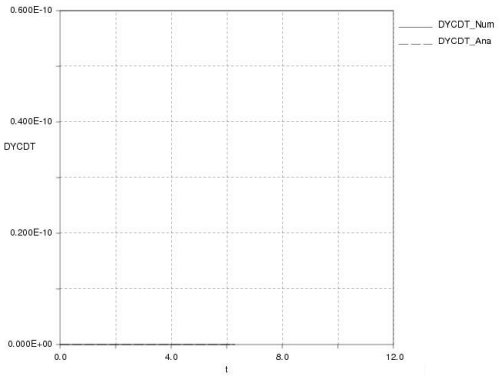

c.

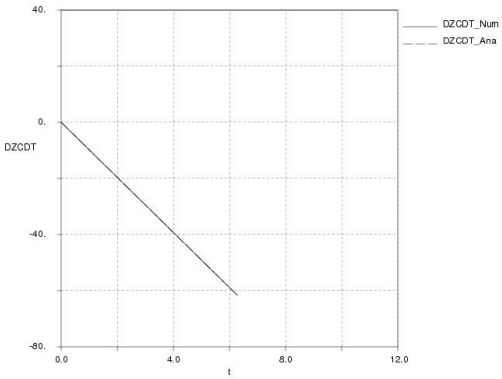

Figure 14. Velocity components of $\dot{x}_C$, $\dot{y}_C$ and $\dot{z}_C$ as functions of time for test case 1.

a.

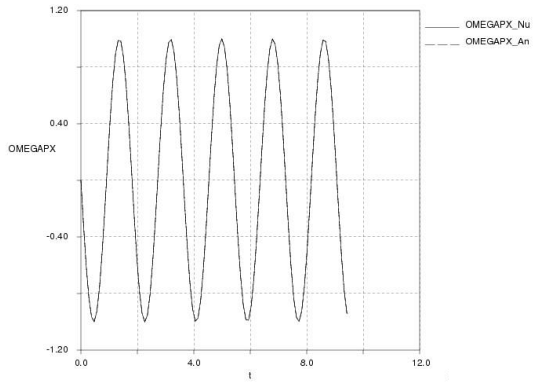

b.

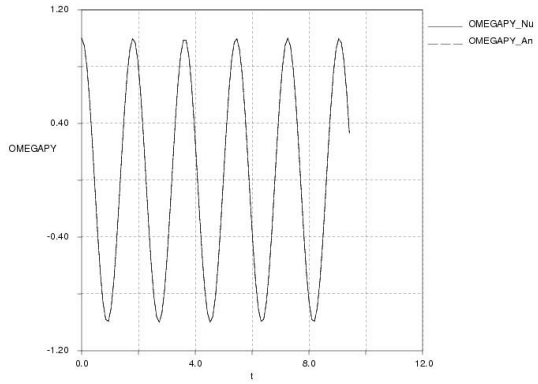

c.

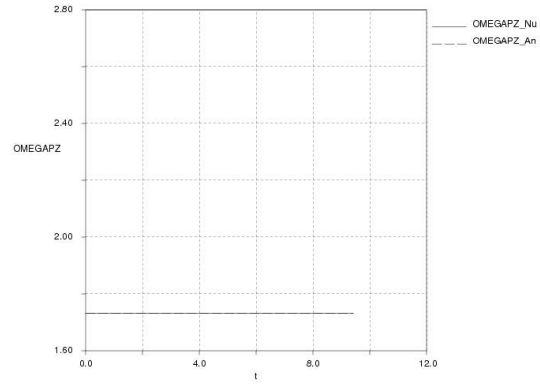

Figure 15. Vorticity vector components of ω_x', ω_y' and ω_z' in the auxiliary coordinate systems as functions of time for test case 2.

a.

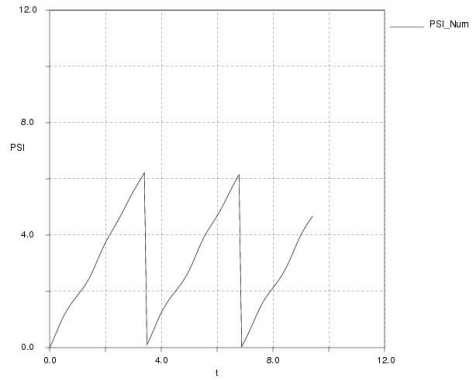

b.

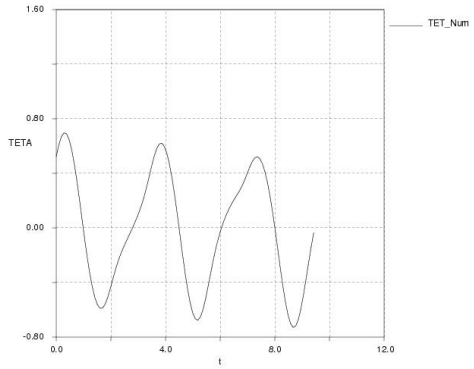

c.

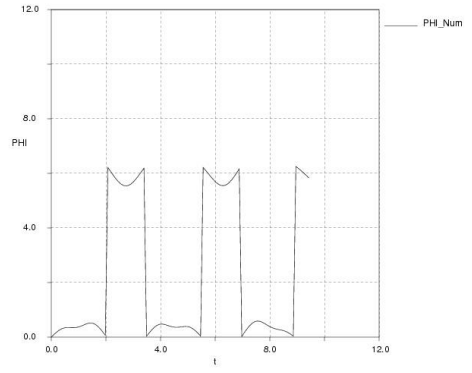

Figure 16. Rotational angles ψ, θ and ϕ as functions of time for test case 1.

a.

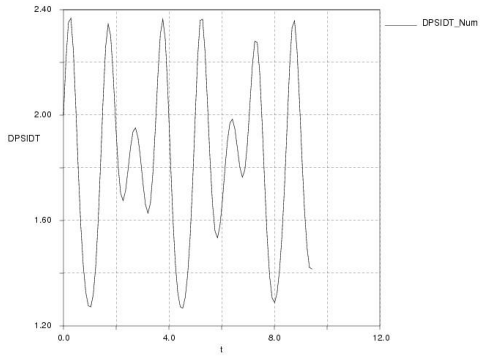

b.

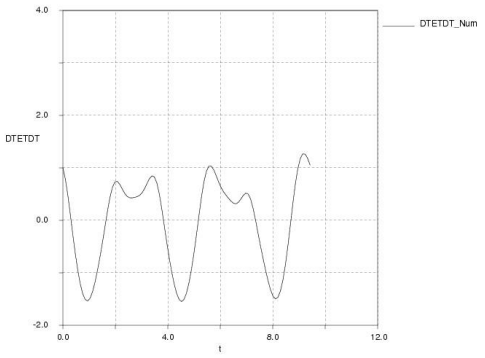

c.

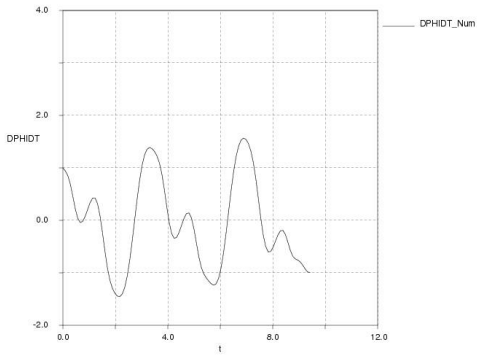

Figure 17. Angular rates $\dot{\psi}, \dot{\theta}$ and $\dot{\phi}$ as functions of time for test case 2.

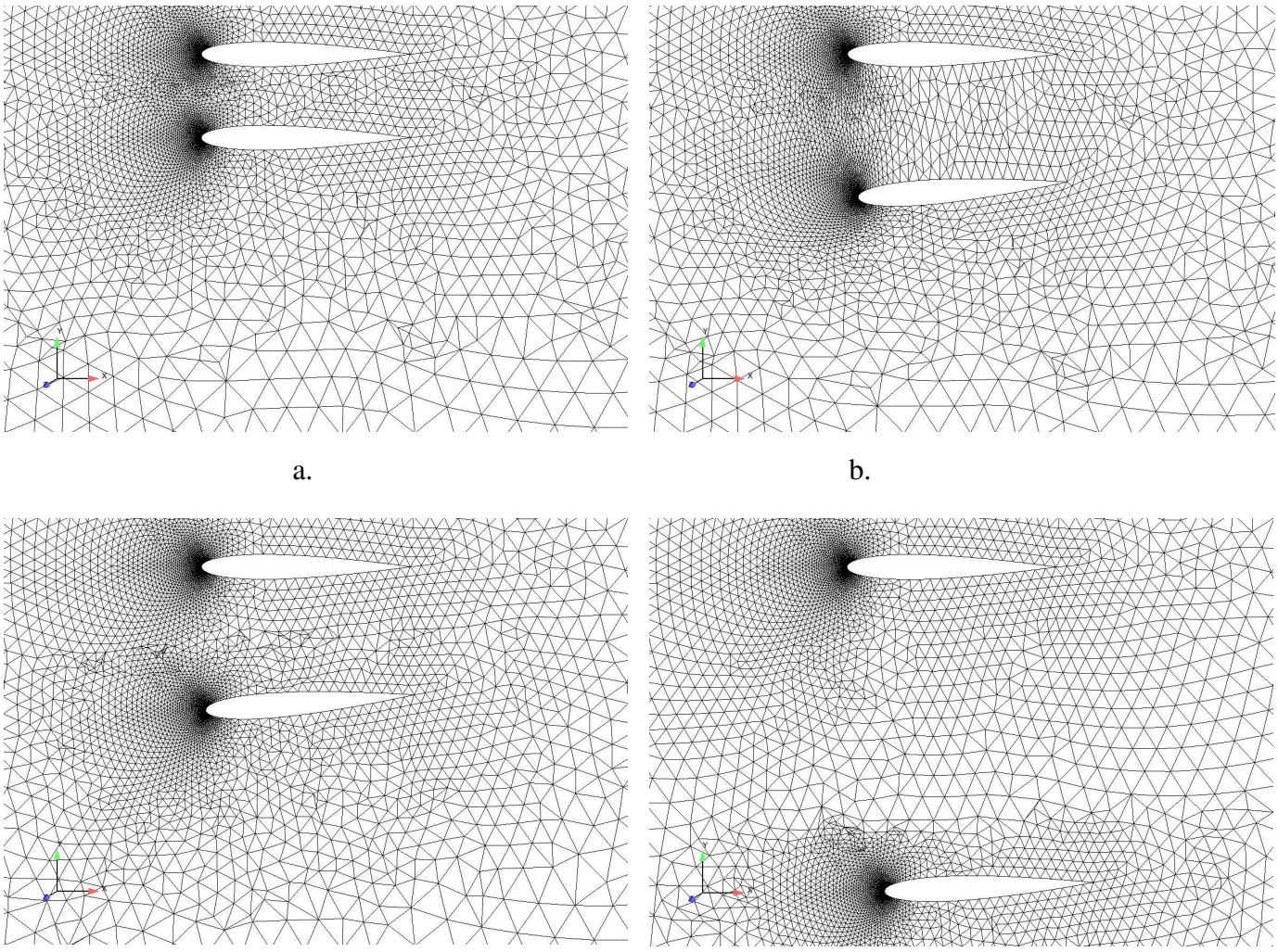

Figure 18. Illustration of the gridding process: a. Initial grid, b. Deformed grid at its final position, c. Remeshed grid in the same position, d. Grid for a position further down .

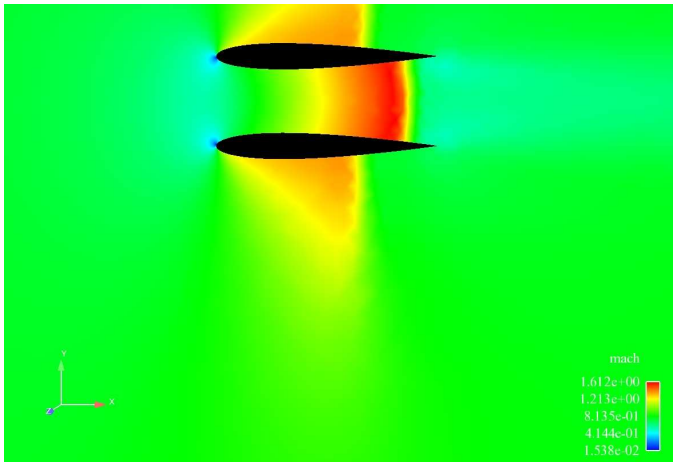

a.

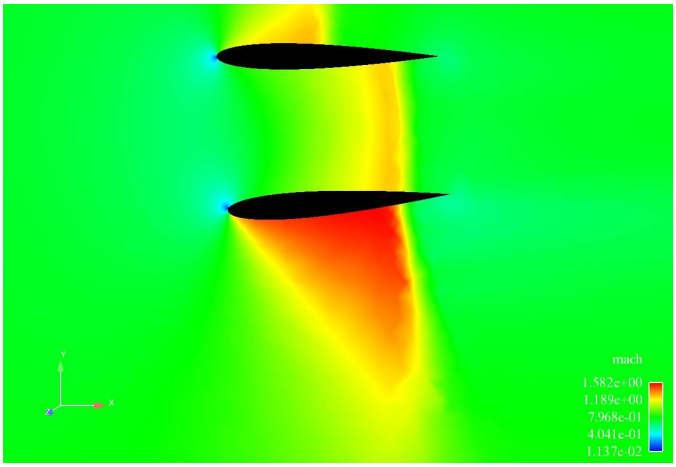

b.

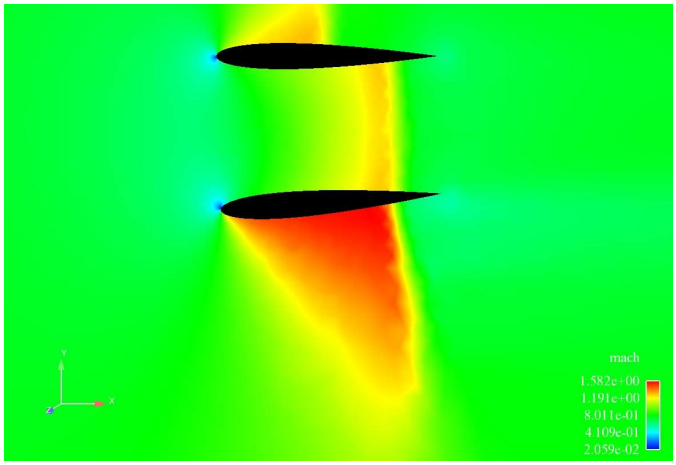

c.

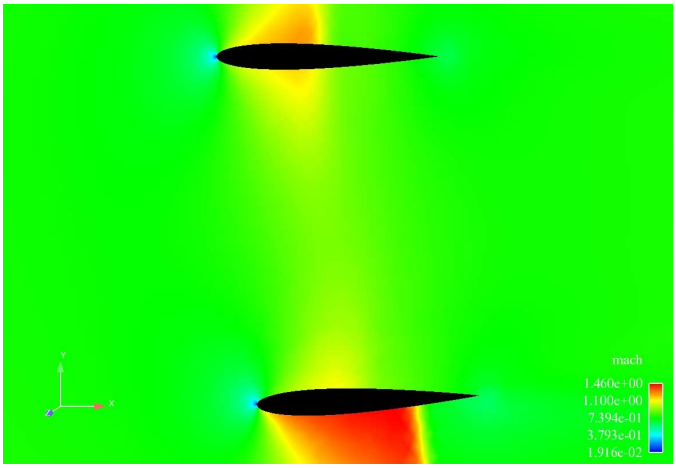

d.

Figure 19. Mach number distribution for the free stream M=0.95 and the angle of attack 0^{o}. The lower wing profile is in the position after t=0.15 sec in a and after t=0.42 sec in b.

a.

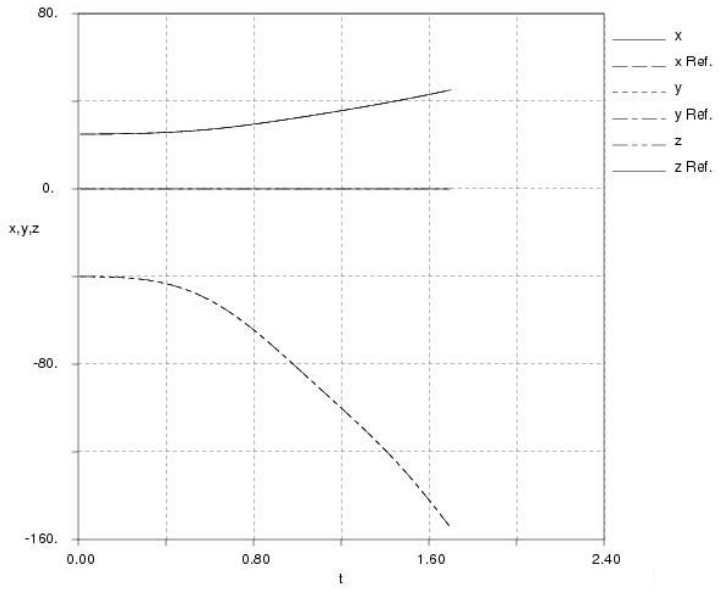

b.

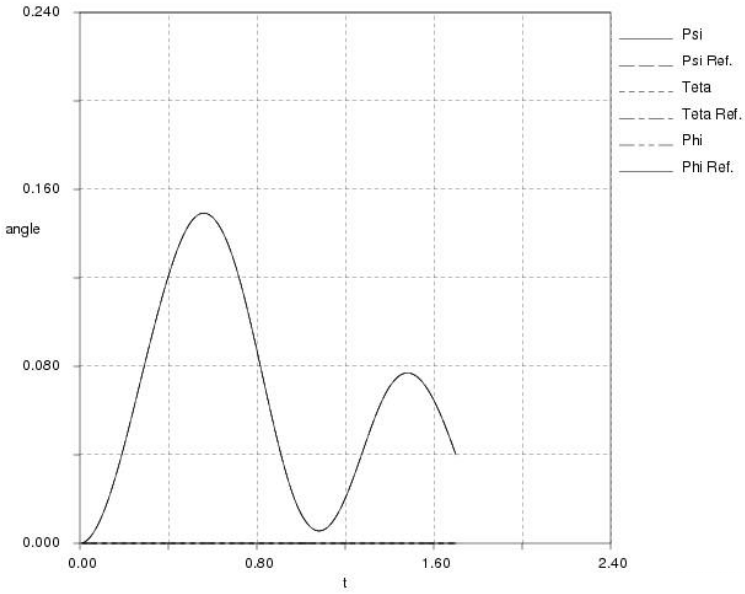

Figure 20.Trajectory and attitude for the wing profile separation test case:

a. Position of mass centre (x_C , y_C , z_C) as functions of time.

b. The rotational angles ψ, θ and ϕ as functions of time.

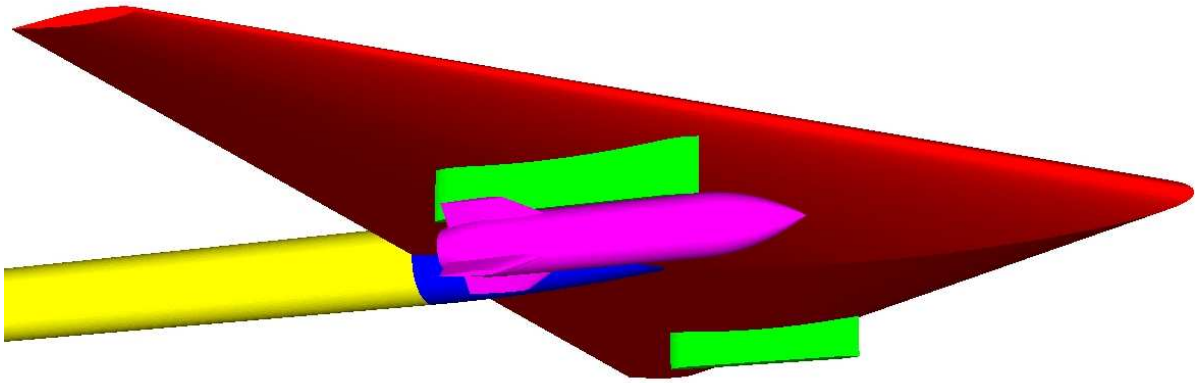

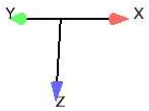

a.

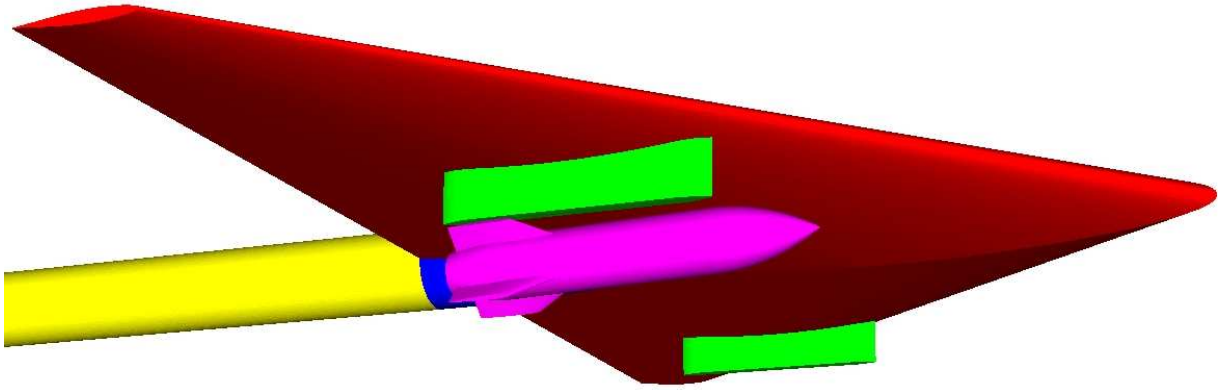

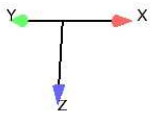

b.

Figure 21. Start position for the finned store: a. in experiments and b. in computations.

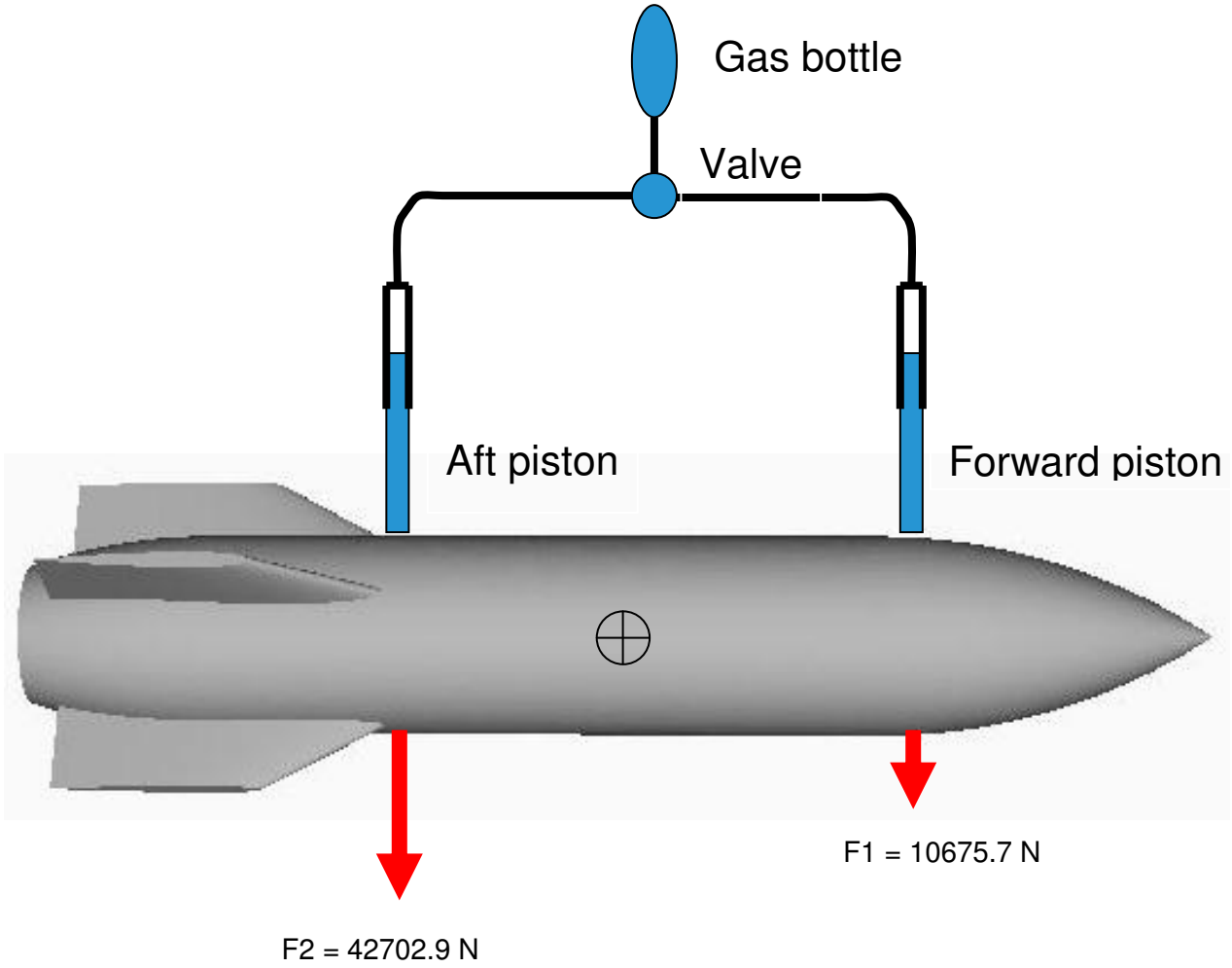

Figure 22. Sketch of the ERU (Ejector Release Unit) . Two pistons with the ejector stroke length 0.10 m is released simultaneously.

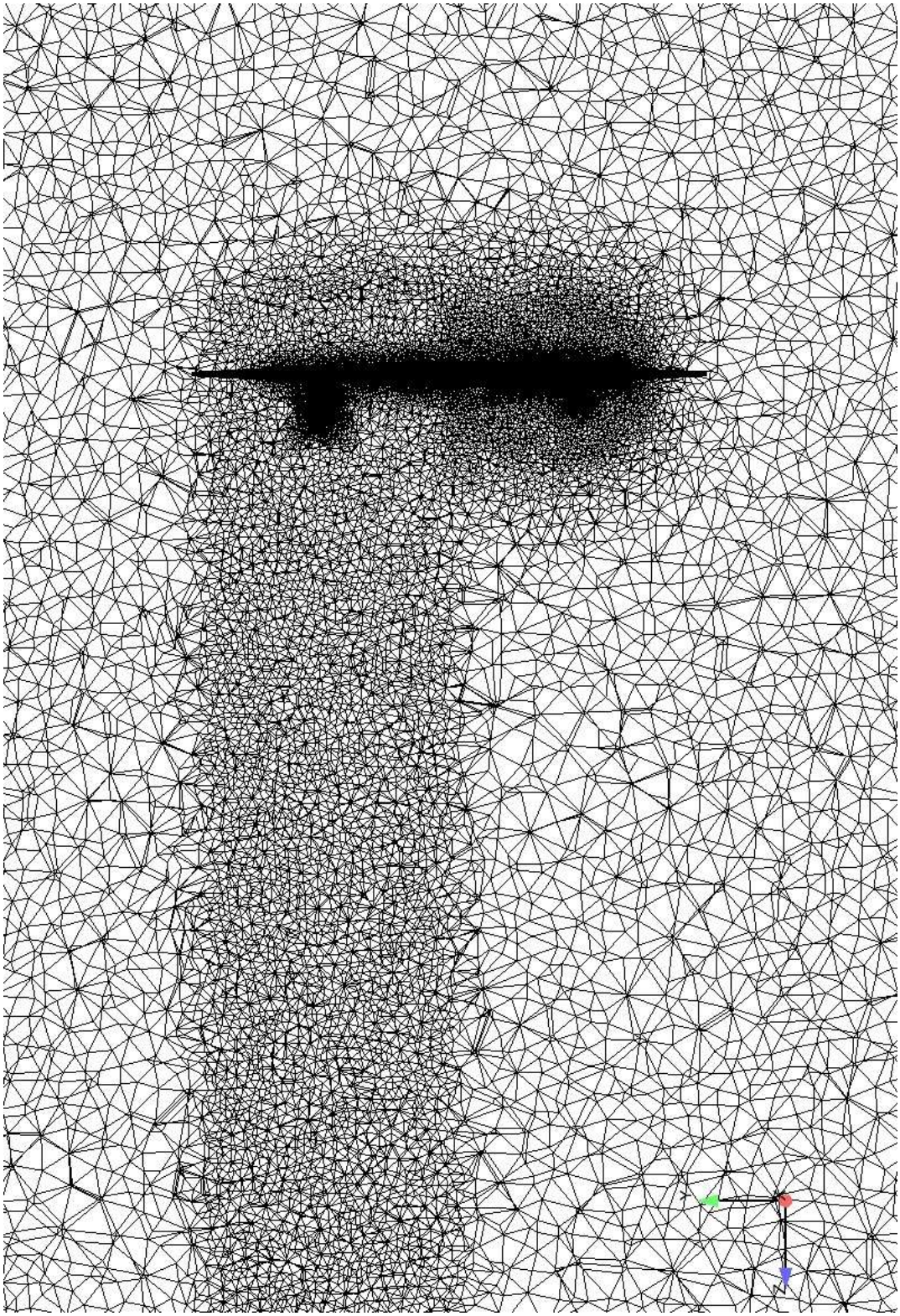

Figure 23. A grid cut through the computational grid seen from in front of the aircraft. The number of nodes is 1765565 grid points.

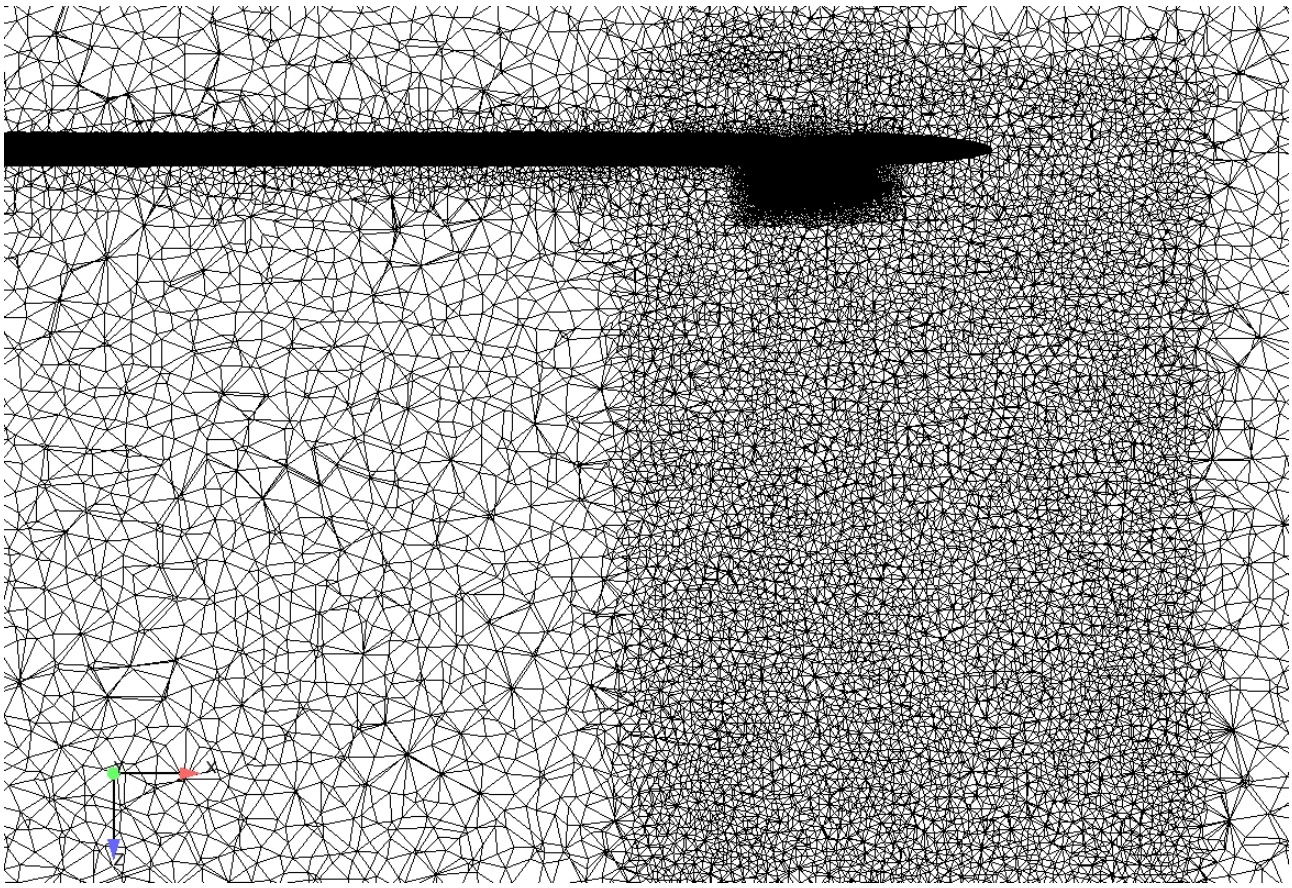

Figure 24. A grid cut through the computational grid seen from the side of the aircraft. The number of nodes is 1765565 grid points.

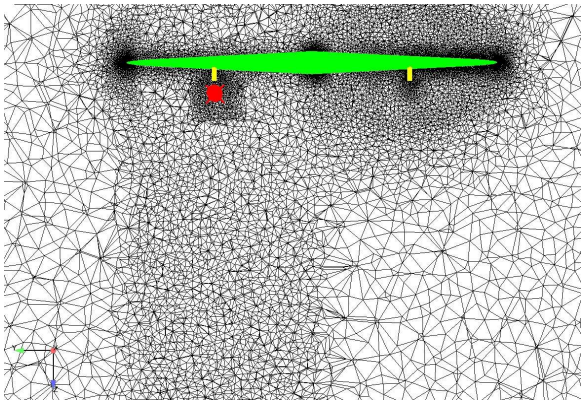

a. t = 0.07 sec

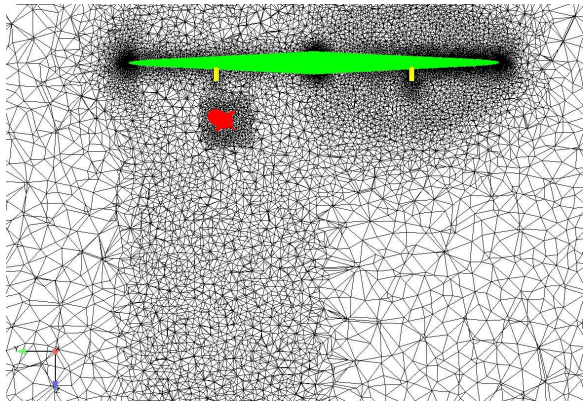

b. t = 0.27 sec

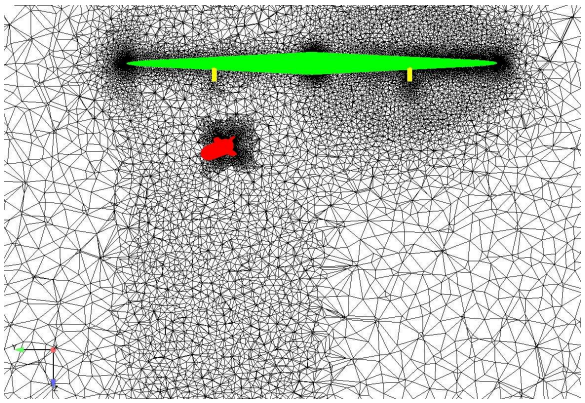

c. t = 0.47 sec

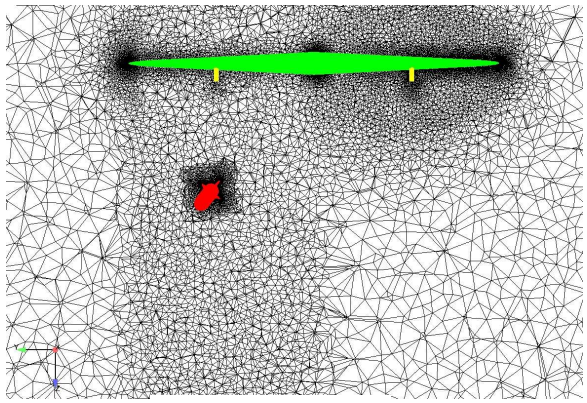

d. t = 0.67 sec

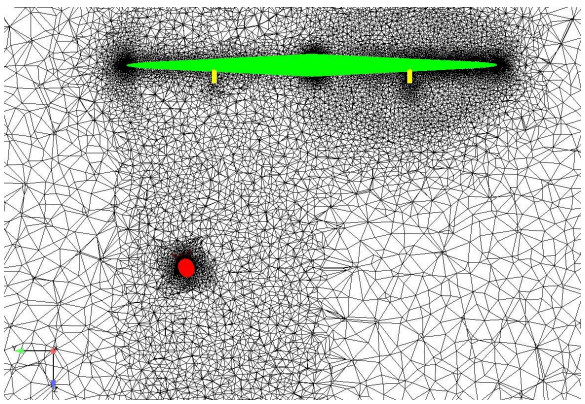

e. t = 0.87 sec

Figure 25. A cut through the merged grid seen from in front of the aircraft.with subsequential positions of the missile.

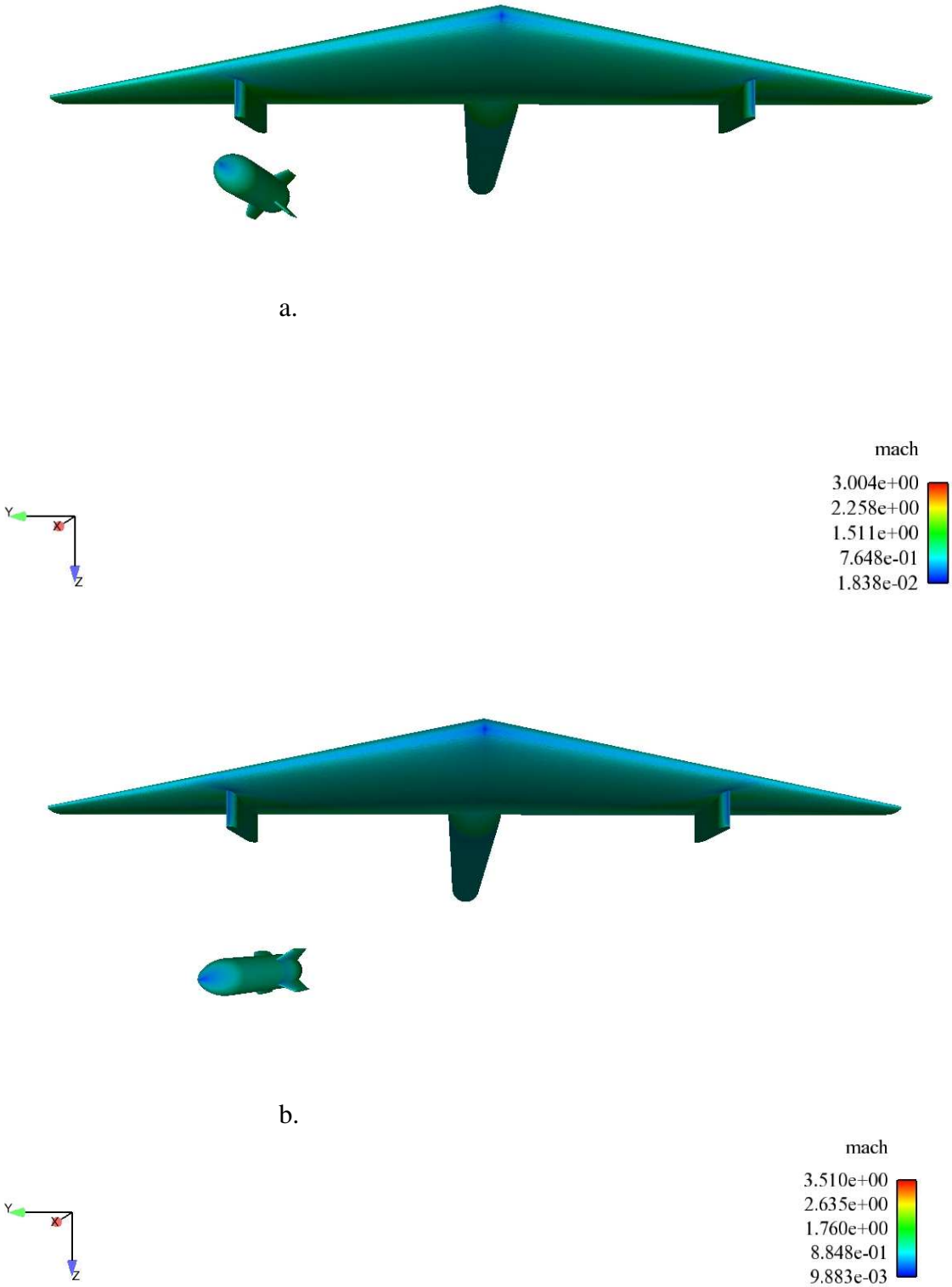

Figure 26. Mach-contours for the case with free stream Mach number M=0.95 and the angle of attack 0°. The store is in the positions after a. t=0.15 sec and after b. t=0.42 sec.

a.

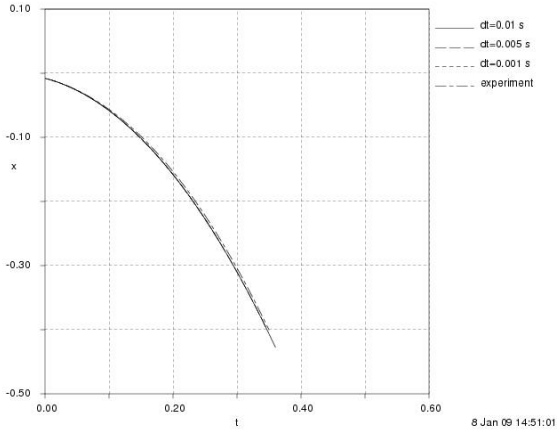

b.

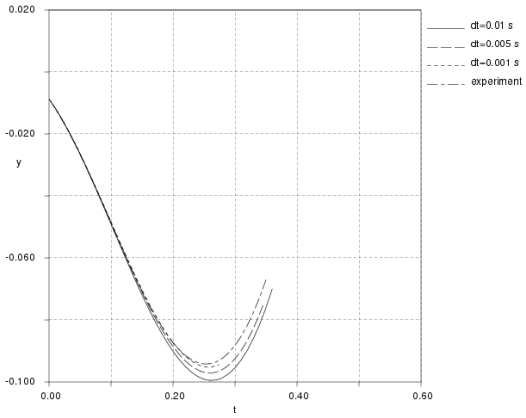

c.

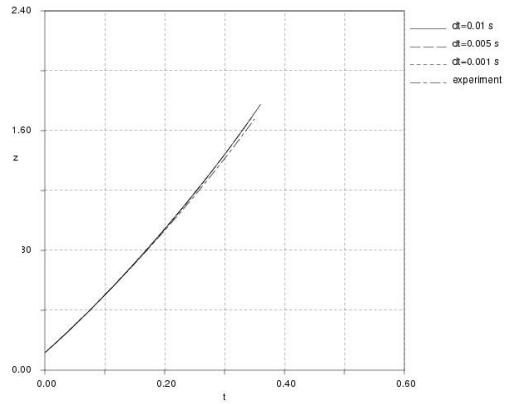

Figure 27. Velocity components of x_C, y_C and z_C as functions of time for the AFRL test case.

a.

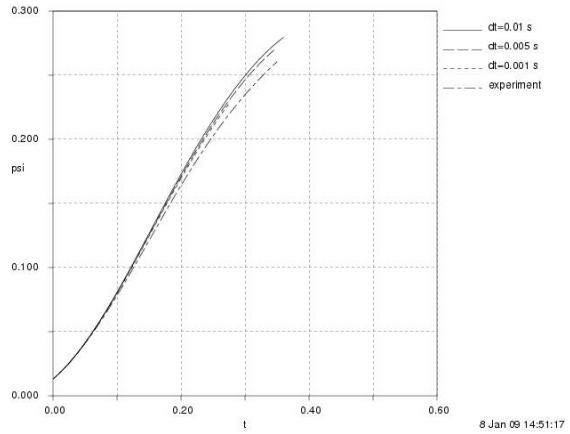

b.

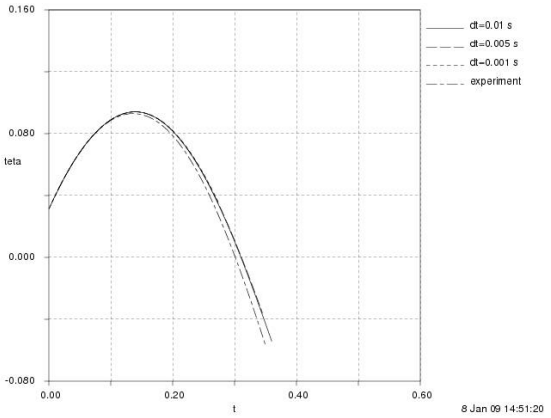

c.

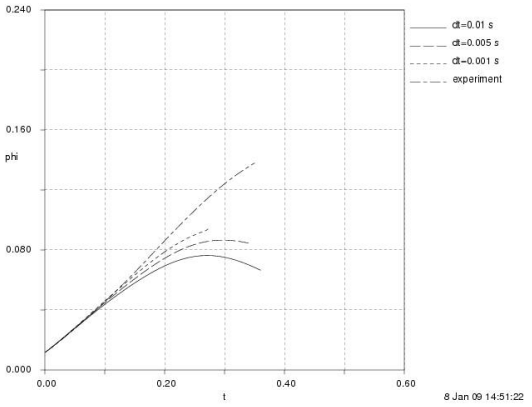

Figure 28. The rotational angles ψ, θ and ϕ as functions of time for the AFRL test case.

a

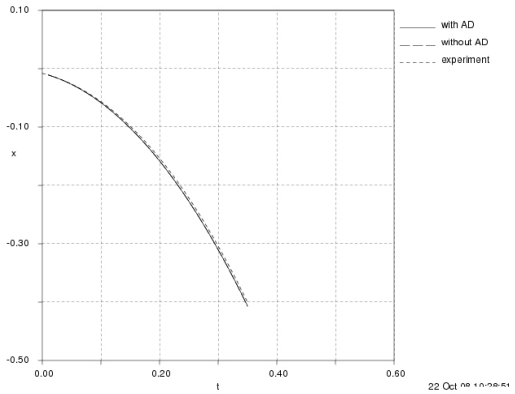

b.

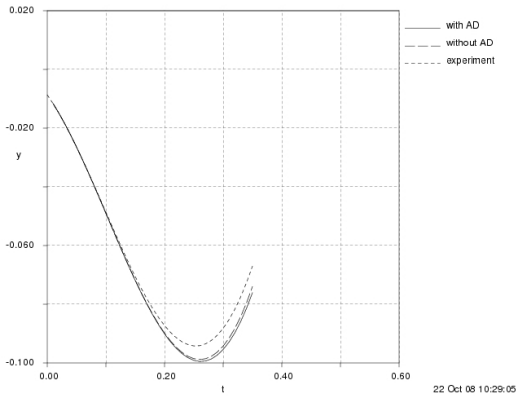

c.

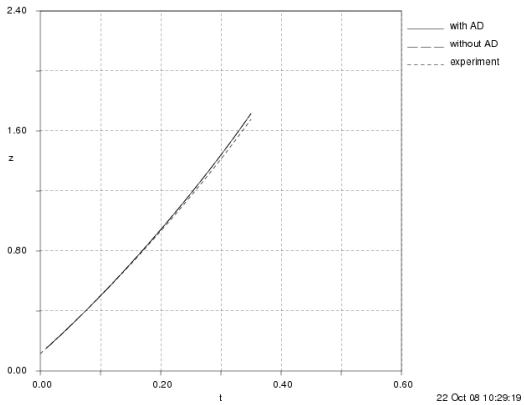

Figure 29. Trajectory components x_C, y_C and z_C with and without aerodynamic damping as functions of time for the AFRL test case.

a.

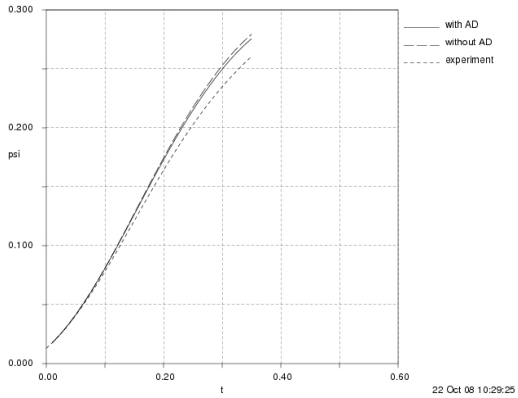

b.

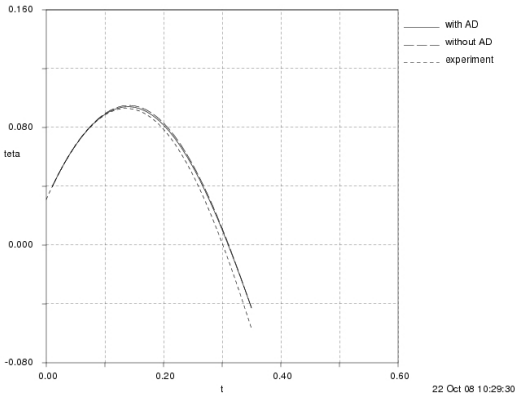

c.

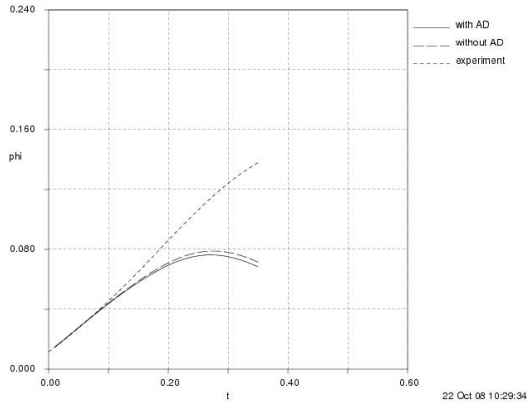

Figure 30. The rotational angles ψ, θ and ϕ as functions of time for the AFRL test case.

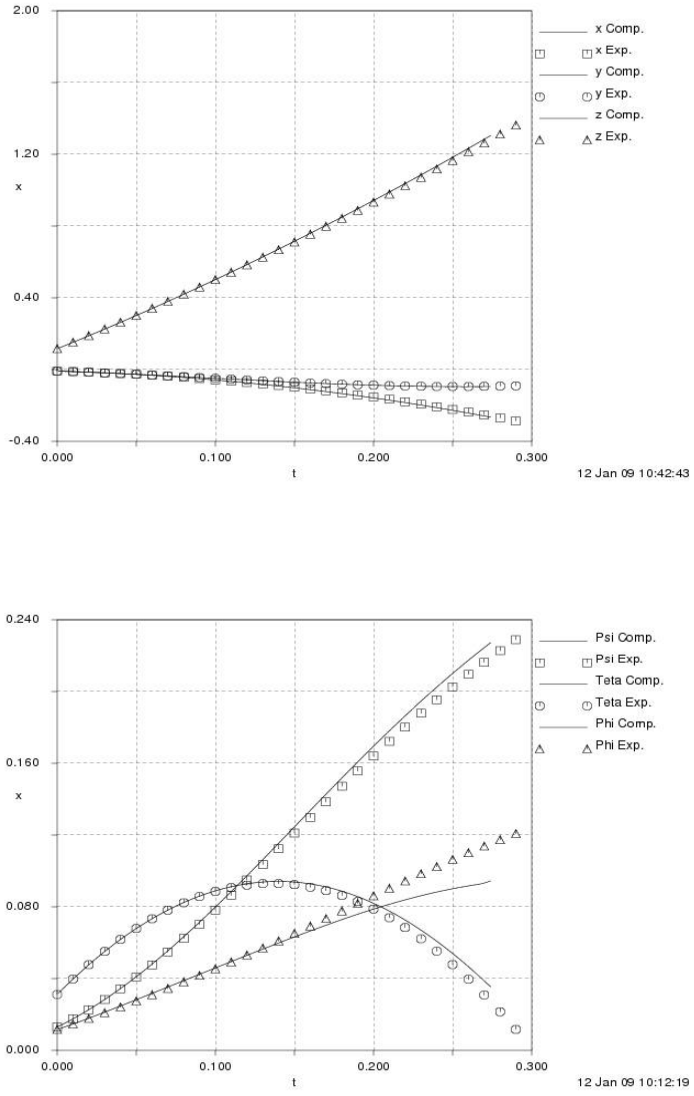

Figure 31. The trajectory and attitude for a quasi-steady Euler computations with $\Delta t = 0.001$ sec.

APPENDIX A

Runge-Kutta method Fehlberg

A fifth order formula using six stages z_{k+1} and a fourth order formula using five stages y_{k+1} are both evaluated.

$$
\begin{aligned}
s_1 &= \Delta t \cdot f(t_k, y_k) \\
s_2 &= \Delta t \cdot f(t + \frac{1}{4}\Delta t, y_k + \frac{1}{4}s_1) \\
s_3 &= \Delta t \cdot f(t + \frac{3}{8}\Delta t, y_k + \frac{3}{32}s_1 + \frac{9}{32}s_2) \\
s_4 &= \Delta t \cdot f(t + \frac{12}{13}\Delta t, y_k + \frac{1932}{2197}s_1 - \frac{7200}{2197}s_2 + \frac{7296}{2197}s_3) \\
s_5 &= \Delta t \cdot f(t + \Delta t, y_k + \frac{439}{216}s_1 - 8s_2 + \frac{3680}{513}s_3 + \frac{845}{4104}s_4) \\
s_6 &= \Delta t \cdot f(t + \frac{1}{2}\Delta t, y_k - \frac{8}{27}s_1 + 2s_2 - \frac{3544}{2565}s_3 + \frac{1859}{4104}s_4 - \frac{11}{40}s_5) \\
y_{k+1} &= y_k + \frac{25}{216}s_1 + \frac{1408}{2565}s_3 + \frac{2197}{4104}s_4 - \frac{1}{5}s_5 \\
z_{k+1} &= y_k + \frac{16}{135}s_1 + \frac{6656}{12825}s_3 + \frac{28561}{56430}s_4 - \frac{9}{50}s_5 + \frac{2}{55}s_6
\end{aligned}
\qquad \text{(A-1)}
$$

The difference $z_{k+1} - y_{k+1}$ is a good estimate of the error in z_{k+1}.

APPENDIX B

Trajectory parameters in the input file

```
*************************************************************************
*                                                                       *
*  ---------------  Trajectory data for moving bodies  ---------------   *
*                                                                       *
*************************************************************************
*                                                                       *
*  ***************  Trajectory data for moving bodies  **************    *
*                                                                       *
TRAJECTORY_DATA,L   ,1,0,6
*                                                                       *
*************************************************************************
*                                                                       *
*  Trajectory solution options                                          *
*   0 = no trajectory computations                                      *
*   1 = quasi steady trajectory computations
*   2 = unsteady trajectory computations
*
*                                                                       *
ITRAJEC,I,1,1,0
1
*************************************************************************
*                                                                       *
*  If ITRAJEC = 1 time step for trajectory computations.
*
*                                                                       *
DELTAT_QS,R,1,1,0
0.01
*************************************************************************
*                                                                       *
*  Gravitational acceleration vector in main frame coordinates          *
*                                                                       *
GRAV,R,3,1,0
0. 0. 9.80665
*************************************************************************
*                                                                       *
*  Number of substeps for 6DoF computations                             *
*                                                                       *
NSUBST,I,1,1,0
10
*************************************************************************
*                                                                       *
*  Parameter controlling the grid check                                 *
*                                                                       *
CHKMAX,R,1,1,0
10.
*************************************************************************
*************************************************************************
*                                                                       *
*  Moving object trajectory data                                        *
*                                                                       *
TRAJECTORY,L   ,1,0,16
*                                                                       *
*************************************************************************
```

```
*****************************************************************************
*                                                                           *
*  Boundary trajectory name                                                 *
*                                                                           *
b_traj_name,L   ,1,1,0
'bomb 1'
*****************************************************************************
*                                                                           *
*  List of object boundary names                                            *
*                                                                           *
b_names,L   ,1,1,0
'STORE<1'
*****************************************************************************
*                                                                           *
*  Object mass                                                              *
*                                                                           *
MASS,R,1,1,0
907.1803317
*****************************************************************************
*                                                                           *
*  The inertia tensor: Ixx,Iyy,Izz,Ixy,Ixz,Iyx                              *
*                                                                           *
INERT,R,6,1,0
27.12 488.1 488.1 0. 0. 0.
*****************************************************************************
*                                                                           *
*  Intitial coordinates of the origo of the auxilary frame in the main      *
*  frame                                                                    *
*                                                                           *
COOR0,R,3,1,0
-0.78892E-02 -0.86864E-02  0.11636E+00
*****************************************************************************
*                                                                           *
*  Coordinates of the position of the store centre of mass in the           *
*  auxilary frame                                                           *
*                                                                           *
COORC,R,3,1,0
0. 0. 0.
*****************************************************************************
*                                                                           *
*  Initial velocity of the store centre of mass in the main frame           *
*                                                                           *
VC0,R,3,1,0
-0.25584E+00 -0.28072E+00  0.35412E+01
*****************************************************************************
*                                                                           *
*  Initial Cardan angles psi, teta, phi in radians                          *
*                                                                           *
CARDAN,R,3,1,0
0.13031E-01  0.31125E-01  0.11603E-01
*****************************************************************************
*                                                                           *
*  Initial Cardan angular rates dpsi/dt, dteta/dt, dphi/dt in radians/s      *
*                                                                           *
CARDANP,R,3,1,0
0.42381E+00  0.89054E+00  0.29571E+00
*****************************************************************************
```

```
*************************************************************************
*                                                                       *
*  Grid compression vector                                              *
*                                                                       *
DEFVEC,R,3,1,0
0. 0. 0.
*************************************************************************
*                                                                       *
*   For quasi steady computations corrections for aerodynamic damping    *
*   is possible                                                          *
*
*                                                                       *
*  Roll damping coefficient                                             *
*                                                                       *
CLP,R,1,1,0
-4.0
*************************************************************************
*                                                                       *
*  Pitch damping coefficient                                            *
*                                                                       *
CMQ,R,1,1,0
-40.0
*************************************************************************
*                                                                       *
*  Yaw damping coefficient                                              *
*                                                                       *
CNR,R,1,1,0
-40.0
*************************************************************************
*                                                                       *
*  Reference length                                                     *
*                                                                       *
RLENGTH,R,1,1,0
0.508
*************************************************************************
*                                                                       *
*  Reference span                                                       *
*                                                                       *
RSPAN,R,1,1,0
0.508
*************************************************************************
*                                                                       *
*  Reference area                                                       *
*                                                                       *
RAERA,R,1,1,0
0.202683
*************************************************************************
```

5 Conclusions

An integrated system for numerical simulation of store separation for quasi-steady flow has been developed and validated. A 6 DOF rigid body-model has been implemented in Edge, FOIs multipurpose flow solver. The grid is deformed in order to conform to the moving boundaries. The computations are coupled to grid generation modules to remesh the grid, if the grid deformation module fails to achieve sufficient grid quality. Typically 10-15 remeshings are required for a store separation trajectory.

Quasi-steady Euler calculations was carried out for an AGARD test case, separation of a finned store from a wing-sting-pylon configuration. The computational results compare well with wind tunnel measurements, except some minor deviation of the roll movement. The flow solver was parallelized at a very late stage of the project, i. e. all the computations showed in this report are carried out on a single processor. This explaines why computations for even smaller time steps were not carried out eventhough there is clear indications that it will improve the results.

The effect of aerodynamic damping was small in this case. In the future, computations of store separation for unsteady flow will be compared with these results. This comparison is of interest since wind tunnel measurements correspond to quasi-steady analysis and flight test corresponds to the unsteady analysis. Furthermore, the viscous forces will have an impact on trajectory and attitude. Modelling of viscous forces is essential to simulate the unsteady flow in weapons bays. In the original project plan the final goal was to develop capability to do trajectory computations for Navier-Stokes computations. It was also planned to do some initial trajectory computations around the FS2020 configuration. However, since the funding of the project was reduced substantially, it was not possible to fulfill these goals.

In order to be able to do Navier-Stokes computations it remains to develop some new functionalities. A routine is needed to mark the nodes in the prismatic layer to avoid deforming the grid in the boundary layer region. Since grid deformation in trajectory computations contexts modifies the grid substantially, especially close to the sensitive region around the store surface, it will be important to retain this part of the grid intact. In order to be able to restart time accurate computations, routines for interpolation of the solution for two previous time levels needs to be developed. Time accurate computations also require fully coupled aerodynamics and flight mechanics calculations, i.e. grid deformations and flight mechanics calculations has to be carried out each subiteration.

The first steps towards a general system for coupling CFD and flight mechanics models has been developed. This new functionality enables computations of a new class of flow problems. Conceivable applications apart from store separation are pilot ejection and specific A/C manoeuvres dominated by non linear aerodynamics.

6 Acknowledgements

This work has been carried out with the support of the Swedish Defence Materiel Administration, FMV. Ingemar Persson at SAAB Aerosystems has been project leader for the FoT25-project: “Studies of Weapons Bays”. The author would like to thank Ingemar Persson and Anders Lindberg at SAAB Aerosystems for interesting discussions and helpful suggestions. The author also wish to acknowledge colleauges at FOI, Peter Eliasson for parallellising the routines for multi-body computations and for reviewing the implementation plan, Oskar Enoksson for writing the shell-scripts for trajectory computations and generation of movies, Lars Tysell for grid generation and adaptation of the routines for remeshing and finally Henrik Edefur for generating the CAD-file and the initial grid files for the AGARD test case.

7 References

[1] Baum J. D., Lou H. and Löhner R.,"A New ALE Adaptive Unstructured Methology for the Simulation of Moving Bodies", AIAA 94-0414(1994).

[2] Lijewski L.and Suhs N.,"Time Accurate Computational Fluid Dynamics Approach to Transonic Store Separartion Trajectory Prediction", Journal of Aircraft, Vol 31, No. 4, July-Aug. 1994.

[3] Coleman L., Jolly B., Chesser B.L. and Brock J., "Numerical Simulation of a Store Separartion Event from an F15-E Aircraft", AIAA 96-3385(1996).

[4] Baum J. D., Lou H., Löhner R., Goldberg E. and Feldhun A., "Application of Unstructured Adaptive Moving Body Methology to the Simulation of Fuel Tank Separation From an F-16C/D Fighter", AIAA-97-0166 (1997).

[5] Stokes S., Chapell J. A.and Letham M,"Efficient Numerical Store Trajectory Prediction For Complex Aircraft/Store Configurations", AIAA 99-3712 (1999).

[6] Dudley J.and Torres J., "Viscous GBU38 Store Separartion from Parent F15E Aircraft During Transonic Flight With Flight Test Comparison", 45th AIAA Aerospace Sciences Meeting and Exhibit, AIAA 2007-72.

[7] Orchard D. M., Lee B. H. K., and Tang F. C., "Influence of Captive Stores on the Unsteady Pressure Distribution within a Rectangular Cavity", ICAS 2008-3.1.3, 2008.

[8] Peng S.-H., "Numerical Analysis of FS2020 Military Aircraft Model with Weapons Bay", FOI-memo-2489-SE, FOI, 2008.

[9] Hallberg E., Lijewski L., Deslandes R., Dillenius M.and Stanek M., "IHAAA Store Separation from Cavity (SSC) Project", ICAS 2008-2.6.3, 2008.

[10] Eliasson P., "Edge, a Navier-Stokes Solver for Unstructured Grids", Proceedings of Finite Volumes applications III, ISBN 1-9039-9634-1, pp. 527-534, 2002

[11] Tysell L., "Implementation of Local Remeshing Routines in Edge", FOI-R-2550-SE.

[12] Goldstein H., "Classical Mechanics", Addison-Wesley Publishing Company, Inc, 1950.

[13] Fox E. A., "Mechanics", Harper and Row Publishers,1967.

[14] Faux I. D. and Pratt M. J.," Computational Geometry for Design and Manufacture", p 72-73, John Wiley & Sons, 1979.

[15] Rice J. R., “Numerical Methods, Software and Analysis”, p 276-277, McGraw-Hill Book Company, 1983.

[16] Etkin B., “Dynamics of Atmospheric Flight”, p 105-145, John Wiley & Sons, 2004.

[17] Lindberg A. “Store separation. An introduction to the methods used at SAAB.”, 2007-03-21, SAAB AeroSystems.

[18] Persson I. and Lindberg A., “Transonic Store Separartion Studies on the SAAB Gripen Aircraft Using Computational Aerodynamics”, ICAS 2008-2.9.1, 2008.

[19] Fox J.H.,”Generic wing pylon, and moving finned store”, Arnold Engineering Development Center(AEDC), Arnold AFB, TN 37389-6001, USA.